**TECHNISCHE
UNIVERSITÄT
DRESDEN**

Holographic description of the equation of state of the quark-gluon plasma

Bachelor-Arbeit
zur Erlangung des Hochschulgrades
Bachelor of Science
im Bachelor-Studiengang Physik

vorgelegt von

JOHANNES KNAUTE

geboren am 22.11.1991 in Dresden

Institut für Theoretische Physik
Fachrichtung Physik
Fakultät Mathematik und Naturwissenschaften
Technische Universität Dresden
2014

Eingereicht am 07. Oktober 2014

1. Gutachter: Prof. Dr. Burkhard Kämpfer
2. Gutachter: Prof. Dr. Dominik Stöckinger

Kurzdarstellung

Im Rahmen der AdS/CFT Korrespondenz wird in dieser Arbeit die Zustandsgleichung des Quark-Gluon Plasmas untersucht. Dazu wird ein holographisches Modell verwendet, welches aus der klassischen Einstein'schen Gravitationstheorie in 5 Dimensionen gekoppelt an ein Skalarfeld mit einem nicht-trivialen Potential besteht. Es werden zwei Potentialansätze analysiert, welche von Kiritsis und Gubser stammen. Die neuesten Daten der Gittereichtheorie für die QCD-Zustandsgleichung werden verwendet, um die Potentialparameter zu fitten. Beim Confinement-Deconfinement Übergang des Quark-Gluon Plasmas handelt es sich um einen sogenannten *crossover*. Um für die Fitprozedur eine Skala festzulegen, werden jeweils Deconfinement Temperaturen T_c definiert. Es wird festgestellt, dass das Kiritsis Modell keine gute Beschreibung der Zustandsgleichung ermöglicht. Auch durch eine Modifikation des Potentials kann keine Verbesserung erreicht werden. Im Gegensatz dazu ermöglicht das Gubser Modell eine gute Reproduktion der Zustandsgleichung im Rahmen der Unsicherheiten der Gitterdaten. Im Temperaturbereich $1 \leq T/T_c \lesssim 3.5$ können die Entropiedichte und der Druck quantitativ sehr gut beschrieben werden. Bei der Schallgeschwindigkeit und dem Wechselwirkungsmaß treten in Abhängigkeit des Fitergebnisses Unterschiede im Hochtemperaturbereich auf.

Abstract

In the context of the AdS/CFT correspondence, the equation of state of the quark-gluon plasma is studied in this work. A holographic model is used, which employs 5-dimensional Einstein gravity coupled to a scalar field with a non-trivial potential. Two potential approaches are analyzed, originating from Kiritsis and Gubser. The most recent data of lattice gauge theory for the QCD equation of state are used to fit the potential parameters. The confinement-deconfinement transition of the quark-gluon plasma is a so-called *crossover*. To set a scale for the fit procedure, deconfinement temperatures T_c are defined respectively. It is found that the Kiritsis model does not allow a good description of the equation of state. Also by a modification of the potential, no improvement can be achieved. In contrast, the Gubser model provides a good reproduction of the equation of state within the uncertainties of the lattice data. In the temperature range $1 \leq T/T_c \lesssim 3.5$ the entropy density and pressure can be quantitatively described very well. With regard to the speed of sound and the interaction measure, differences occur in the high temperature range depending on the fit result.

Contents

1 Introduction

In the early universe, a transition from the quark-gluon plasma, i.e. a deconfined phase dominated by colored degrees of freedom, to a confined phase (color neutral hadrons) occurred. Nowadays, this transition can be reproduced in heavy ion collisions at the Large Hadron Collider (LHC, CERN). The fundamental theory, which describes these strong interactions between quarks and gluons is Quantum Chromodynamics (QCD). An important research aim is the accurate description of the QCD phase diagram and the thermodynamics of strongly interacting matter. Lattice gauge theory is an established method for such non-perturbative effects. A new method is the Anti de Sitter - Conformal Field theory (AdS/CFT) correspondence, which was discovered by Maldacena in 1997. This correspondence relates quantum field theories with conformal invariance (living in our flat 4-dimensional space) and string theory. The latter one is a quantum theory of gravity and a promising candidate for the consistent quantization of gravity. Strong CFT coupling is translated into weak string coupling and vice versa. In a certain limiting case, the AdS/CFT correspondence describes the duality between a CFT and a classical theory of gravity. In fact, QCD is not a CFT. However, the quark-gluon plasma at high energies can be approximately described by a CFT. Therefore, the correspondence may be employed.

In this thesis, the duality of a 5-dimensional gravity theory and a quantum field theory in 4 dimensions is applied, to study the strongly coupled quark-gluon plasma. Since the field theory lives at the boundary of the higher dimensional gravity theory, one speaks also of a *holographic principle*. It is the goal of this thesis to reproduce the equation of state of the quark-gluon plasma from the lattice results.

The thesis is organized as follows. In chapter 2 we describe the necessary theoretical principles. At first, the fundamentals of general relativity are described. Afterwards, Quantum Chromodynamics is introduced. We focus on the properties and the Lagrangian formulation of Yang-Mills theories. The QCD phase diagram is described. The relevant elements of string theory are discussed. The AdS/CFT correspondence is introduced in section 2.4. The Anti de Sitter space and conformal field theories are defined. Different variants and the validity of the correspondence are discussed. We give a brief introduction into the state map of the holographic principle. In chapter 3, we evaluate the lattice gauge theory results, since the holographic models are fitted to the data. Chapter 4 deals with these holographic models.

We consider two potential approaches, namely the models from Kiritsis and Gubser. The fit procedure is described for the reconstruction of the QCD equation of state. The fit results are discussed in comparison to the lattice results.

Appendix A is devoted to some more detailed calculations of the Gubser model. Appendix B is a treatise, which summarizes previous studies in which we have described the pure gluon plasma holographically.

2 Theoretical principles

2.1 General relativity

General theory of relativity (GTR) is a relativistic generalization of the Newtonian theory of gravitation [1]. Because the gravitational field contains energy, it represents itself a source of the field. The first hypothesis, which underlies GTR, is that the metric in the four-dimensional event space is pseudo-Riemannian [2]. There are coordinates $(x^0, \vec{x})$, in which the metric tensor $g_{\mu\nu}$ and the first fundamental form have the following form

$$ds^2 = g_{\mu\nu} dx^\mu dx^\nu \ . \tag{2.1}$$

In an infinitesimal neighborhood of a point on the manifold the relation $g_{\mu\nu} = \eta_{\mu\nu} + \gamma_{\mu\nu}$ holds, where $\eta_{\mu\nu}$ is the Euclidean metric and the coefficients fulfill the condition $|\gamma_{\mu\nu}| \ll 1$. The energy-momentum tensor $T^{\mu\nu} = T^{\mu\nu}(x^0, \vec{x})$ describes the motion and distribution of matter in spacetime except those arising from the gravitational field. The component T^{00} represents the energy density. In analogy to the law of conservation of energy and momentum in special relativity, it is required that the tensor $T^{\mu\nu}$ is covariantly conserved

$$\nabla_\mu T^{\mu\nu} \equiv T^{\mu\nu}_{\ \ ;\mu} = 0 \ . \tag{2.2}$$

Here, ∇_μ represents the absolute or covariant derivative. In an arbitrary coordinate system this relation does not imply a global conservation law of energy or momentum in general. The second fundamental hypothesis in general relativity is that the energy-momentum tensor is given by the pseudo-Riemannian geometry itself. The simplest tensor that fulfills condition (2.2) is the so-called Einstein tensor $G_{\mu\nu} \equiv R_{\mu\nu} - \frac{R}{2} g_{\mu\nu}$. Here, $R_{\mu\nu}$ is the Ricci tensor and R the Ricci scalar. This results in a direct proportionality between $G_{\mu\nu}$ and $T_{\mu\nu}$. The proportionality constant κ describes the coupling between matter and spacetime curvature. Written with the cosmological constant Λ one obtains the Einstein field equations

$$G_{\mu\nu} + \Lambda g_{\mu\nu} \equiv R_{\mu\nu} - \frac{R}{2} g_{\mu\nu} + \Lambda g_{\mu\nu} = \kappa T_{\mu\nu} \ . \tag{2.3}$$

In a four-dimensional space κ is related to Newton's gravitational constant G via $\kappa = \frac{8\pi G}{c^4}$. The equations of motion for a point-like particle of mass m are

$$m\frac{d^2 x^\mu}{d\tau^2} + m\Gamma^\mu_{\alpha\beta}\frac{\partial x^\alpha}{\partial \tau}\frac{\partial x^\beta}{\partial \tau} = K^\mu \tag{2.4}$$

with τ as a affine curve parameter, $\Gamma^\mu_{\alpha\beta}$ as the Christoffel symbol of the second kind and K^μ as a non-gravitational force. If $K^\mu = 0$, the world line of a point particle is a geodesic in spacetime. Thus, the tensor $T_{\mu\nu}$ is related to the gravitation field (which determines the course of the geodesics for point particles) through the pseudo-Riemannian metric [2].

Einstein's field equations (2.3) can also be derived from an extremum principle with the Euler-Lagrange equations. The corresponding action is (see [3] for the original work from Hilbert or [4,5] for detailed discussions)

$$S = S_F + S_M = \int d^4 x \sqrt{-g}\left[\frac{R}{2\kappa} + \mathcal{L}_M(A, g_{\mu\nu})\right] . \tag{2.5}$$

S_F denotes the action for the free gravitational field and S_M stands for the action of the matter field, where A contains all „matter variables" and $g \equiv \det(g_{\mu\nu})$. Requiring $\delta S = 0$ yields at first $2\kappa\delta S_F = \int d^4 x\left[(\delta g^{\mu\nu})R_{\mu\nu}\sqrt{-g} + g^{\mu\nu}(\delta R_{\mu\nu})\sqrt{-g} + R(\delta\sqrt{-g})\right] = 0$. Using $\delta\sqrt{-g} = -\frac{1}{2\sqrt{-g}}\delta g = -\frac{\sqrt{-g}}{2}g_{\mu\nu}\delta g^{\mu\nu}$, one obtains

$$2\kappa\delta S_F = \int \left(R_{\mu\nu} - \frac{1}{2}g_{\mu\nu}R\right)\delta g^{\mu\nu}\sqrt{-g}d^4 x + \int g^{\mu\nu}\delta R_{\mu\nu}\sqrt{-g}d^4 x \qquad \forall \delta g^{\mu\nu} . \tag{2.6}$$

The second term vanishes because it can be converted to a surface integral by using Stokes integral theorem. Thus, the requirement $2\kappa\delta S_F = 0$ leads to $G_{\mu\nu} = 0$. The variation of S_M w.r.t. to the matter variables leads to the matter field equations

$$\frac{\partial \mathcal{L}_M}{\partial A} - \partial_\mu \frac{\partial \mathcal{L}_M}{\partial A_{,\mu}} = 0 . \tag{2.7}$$

The variation according to $g^{\mu\nu}$ yields

$$\delta S_M = \int d^4 x\left[\frac{\partial(\mathcal{L}_M\sqrt{-g})}{\partial g^{\mu\nu}}\delta g^{\mu\nu} + \frac{\partial(\mathcal{L}_M\sqrt{-g})}{\partial g^{\mu\nu}_{,\kappa}}\delta g^{\mu\nu}_{,\kappa}\right] = \int d^4 x\sqrt{-g}\frac{1}{2}T_{\mu\nu}\delta g^{\mu\nu} \tag{2.8}$$

whereby

$$T_{\mu\nu} := \frac{2}{\sqrt{-g}}\frac{\delta(\mathcal{L}_M\sqrt{-g})}{\delta g^{\mu\nu}} = \frac{2}{\sqrt{-g}}\left[\frac{\partial(\mathcal{L}_M\sqrt{-g})}{\partial g^{\mu\nu}} - \partial_\kappa\frac{\partial(\mathcal{L}_M\sqrt{-g})}{\partial g^{\mu\nu}_{,\kappa}}\right] \tag{2.9}$$

defines the energy-momentum tensor of the matter. $T_{\mu\nu}$ is symmetric and, due to the Bianchi identity, $T^{\mu\nu}_{\ ;\mu} = 0$ holds. Since a constant Λ can be added in the action, this results in the field equations (2.3).

2.2 Quantum Chromodynamics

2.2.1 Properties

Quantum chromodynamics (QCD) describes as a quantum field theory (QFT) strong interactions [6]. It is a non-abelian local gauge theory with symmetry group SU(3). QCD deals with quarks - massive spin-$\frac{1}{2}$ fermions with a color charge whereas gluons are the interaction particles. (These are spin-1 bosons that also carry color charges.) In contrast to quantum electrodynamics (QED) gluons can interact with each other. Furthermore, the coupling decreases with increasing energy or momentum [7]. This leads to the asymptotic freedom for high energies or momenta: This means that quarks and gluons behave, at small distances, like free particles and interact weakly. Previously, it was believed that the formation of a quark-gluon plasma (QGP) is related to asymptotic freedom. It happens, however, that deconfinement with nearly free quarks and gluons is related also to non-perturbative effects. For low energies confinement occurs. This refers to the fact that the force between quarks (and gluons) does not diminish if the distance between them enlarges. Hadronisation denotes the formation of colorless mesons and baryons when quarks are separated [7]. In this case, quarks are always bound together into hadrons. Thus, the quark confinement postulate is the same as that of the non-observability of colored states [6]: All hadron states and physical observables are color-singlets.

2.2.2 Yang-Mills theories and Lagrangian

The following section shall give a short introduction into the Lagrangian formalism of QCD as a quantized non-abelian gauge field theory. It is based on [6].

Yang-Mills theory is obtained by extending the algebra of QED to a more general noncommutative (non-abelian) algebra. Let us consider a quark field $\psi(x)$ with mass m which belongs to the N-dimensional fundamental representation of the group G (later this will be particularly the color group SU(3)). G can be restricted to semi-simple Lie groups. The corresponding Lie algebra is generated by n generators T^a, $a = 1, 2, \ldots, n$ which fulfill the commutation relations $[T^a, T^b] = if^{abc}T^c$, where f^{abc} are the structure constants. The transformation property of $\psi(x)$ under the operation of the group element U of G is given by

$$\psi'_i = U_{ij}\psi_j \;, \qquad U = \exp(-iT^a\theta^a) \tag{2.10}$$

with $\theta^a = \theta^a(x)$ as parameters. We use the following ansatz for the covariant derivative to construct an invariant Lagrangian under local gauge transformations

$$D_\mu = \partial_\mu - igT^aA^a_\mu \;, \tag{2.11}$$

where A_μ^a are gauge fields and g is the coupling representing the interaction strength between ψ and A_μ^a. Then, the Lagrangian for the fermion field $\psi(x)$ in interaction with the gauge fields is given by $\mathcal{L} = \bar{\psi}(i\gamma^\mu D_\mu - m)\psi$ with m as the mass parameter. It can be shown that $\mathcal{L}$ is invariant under (2.10) if A_μ^a obeys the transformation rule

$$T^a A_\mu'^a = U(T^a A_\mu^a - \frac{i}{g}U^{-1}\partial_\mu U)U^{-1} \ . \tag{2.12}$$

In analogy to QED one can show $[D_\mu, D_\nu] = -igT^a F_{\mu\nu}^a$ with $F_{\mu\nu}^a$ as the field strength for the non-abelian gauge fields, defined by

$$F_{\mu\nu}^a \equiv \partial_\mu A_\nu^a - \partial_\nu A_\mu^a + g f^{abc} A_\mu^b A_\nu^c \ . \tag{2.13}$$

It can be shown that the term $F_{\mu\nu}^a F^{a\mu\nu}$ is gauge invariant. Thus, the final form of the Lagrangian which is invariant under (2.10) and (2.12) is

$$\mathcal{L} = -\frac{1}{4}F_{\mu\nu}^a F^{a\mu\nu} + \bar{\psi}(i\gamma^\mu D_\mu - m)\psi \ . \tag{2.14}$$

The gauge coupling g and the mass m are the parameters for the gauge principle. This principle includes Lorentz invariance and invariances under space and time reversal. However, (2.14) is not unique. It is important to note that the Lagrangian includes self-interactions of the gauge fields (gluons in QCD) through the last term in (2.13). This causes mainly the asymptotic freedom. Particularly in QCD, G corresponds to the color SU(3). Quarks ψ belong to the fundamental and gluons A_μ^a to the adjoint representations. In QCD, the classical Lagrangian is given by

$$\mathcal{L}_{QCD} = -\frac{1}{4}F_{\mu\nu}^a F^{a\mu\nu} + \sum_{k=1}^{N_f} \bar{\psi}^k(i\gamma^\mu D_\mu - m)\psi^k \tag{2.15}$$

where the sum over k involves all quark flavors and $a = 1, 2, \ldots, 8$.

2.2.3 The QCD phase diagram

The QCD phase diagram covers different phases of strongly interacting matter as a function of temperature T and baryo-chemical potential μ_B as sketched in figure 2.1. A first prototype was conjectured in [9]. The current research is still far remote from a complete understanding of the QCD thermodynamics. However, this section gives a summary of the established phases. The discussion follows [10].

For low T and μ_B, quarks and gluons exist only as colorless bound states, i.e. hadrons and pure glueballs. Thus, in this region confinement is present (see also section 2.2.1 for properties). For high T and/or high μ_B, the deconfined QGP occurs. Quarks and gluons as the degrees of freedom interact strongly. Obviously, there is a deconfinement transition between those
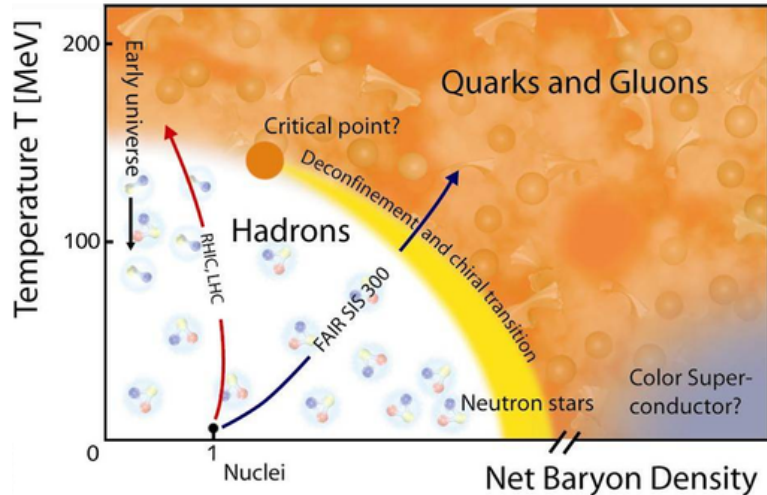
Figure 2.1: The QCD phase diagram, taken from [8].

two phases. For low μ_B, it is a crossover at a confinement scale $T_c \approx 150 - 170\,\text{MeV}$ [11, 12], while for higher μ_B a first-order phase transition is assumed that probably starts in a critical point. Furthermore a chiral phase transition is expected, during which the chiral symmetry of the QCD-Lagrangian is spontaneously broken [13]. Details of the phase diagram and the transition curves are still matter of debate, e.g. also the phases for higher μ_B and lower T.

Heavy-ion collisions are the most important experimental method for studying QCD thermodynamics. Current facilities are the LHC or RHIC, a future facility is FAIR[1] (see figure 2.1 for their range in the phase diagram). During a heavy-ion collision, the particles interact strongly and form a QGP fireball. While expanding, the plasma cools and reaches the transition area. Then, quarks and gluons confine and form a gas of hadron resonances [10]. The resonances freeze out and decay products are emitted, which might be detected. The hadrons are also subject to the electromagnetic or weak interaction in the final state. There occur also direct probes of the fireball such as real and virtual photons.

2.3 String theory

The following section shall give a short introduction into the main concepts of string theory that are important for AdS/CFT correspondence. It is mainly based on [14] and [15]. For an extensive summary see e.g. [16].

String theory is the theory of relativistic strings i.e. a generalization of QFT whereby the fundamental objects are extended, one-dimensional lines or loops. Strings can have a tension (energy per unit length). Thus, the only possible action is the one whose variational law minimizes the total area of the string worldsheet (surface swept out by the moving string) in

---

[1]Large Hadron Collider at CERN, Relativistic Heavy Ion Collider at the Brookhaven National Laboratory and Facility for Antiproton and Ion Research at GSI in Darmstadt

spacetime. In a first step, we consider the bosonic string. Let $X^\mu(\sigma, \tau)$ be the coordinates for the string position (σ: worldsheet length, τ: worldsheet time). The Nambu-Goto action is

$$S_{NG} = -T \int d\sigma d\tau \sqrt{\det(h_{ab})} \, , \tag{2.16}$$

where $T = \frac{1}{2\pi\alpha'}$ is the string tension, connected via $\alpha' = l_s^2$ to the intrinsic string length, and $h_{ab} = \partial_a X^\mu \partial_b X^\nu g_{\mu\nu}(X)$ is the induced spacetime metric. The Nambu-Goto action allows the calculation of the string trajectory through spacetime. A more fundamental form is the Polyakov action

$$S_P[X, \gamma] = -\frac{T}{2} \int d\sigma d\tau \sqrt{-\gamma} \gamma^{ab} h_{ab} \, . \tag{2.17}$$

Here, γ^{ab} has the interpretation as an independent metric on the worldsheet. Note that quantum mechanically the two actions are not the same, because the Polyakov action has more symmetries.[2] Using the equation of motion with respect to γ^{ab}, one can show the coincidence with (2.16). Essentially, one needs to define boundary conditions for strings. An open string can have Neumann (free endpoints) or Dirichlet (fixed endpoints) boundary conditions.

The action can be easily generalized to a p-brane action, i.e. a p-brane sweeping out a $(p+1)$-dimensional world volume in D-dimensional spacetime. The action takes the form

$$S_p = -T_p \int d\mu_p \, , \tag{2.18}$$

whereby T_p is the p-brane tension and $d\mu_p$ the $(p + 1)$-dimensional volume element, given by $d\mu_p = \sqrt{-\det G_{\alpha\beta}} d^{p+1}\sigma$ with $G_{\alpha\beta} = g_{\mu\nu}(X)\partial_\alpha X^\mu \partial_\beta X^\nu$, $(\alpha, \beta = 0, \ldots, p)$. Fixing a gauge reduces the closed string action to free 2-dimensional bosons. The solution of the wave equation (that is yielded by the X^μ equation of motion) contains left and right moving wave modes. The open string mode expansion has standing waves for its solution.

The next step is to apply the canonical quantization to the worldsheet field theory under consideration of physical state conditions. This yields the particle spectrum: massless particles are the graviton, an antisymmetric tensor and a scalar (dilaton). Quantum consistency requires the dimension $D = 26$. Strings can interact with each other and the strength of the interaction is governed by the string coupling g_s.

Since the bosonic string is unstable (there is a tachyonic ground state), one introduces a superstring (i.e. a supersymmetric string). In general, there are two ways to introduce supersymmetry in string theory: On one hand, the *Ramond-Neveu-Schwarz (RNS) formalism* uses two-dimensional worldsheet supersymmetry. A different way is the *Light-Cone Green-Schwarz*

---

[2]Indeed, the Weyl invariance is not present in the Nambu-Goto action. The worldsheet Weyl invariance is defined by $X'^\mu(\sigma, \tau) = X^\mu(\sigma, \tau)$, $\gamma'_{ab}(\sigma, \tau) = \exp\{2\omega(\sigma, \tau)\} \gamma_{ab}(\sigma, \tau)$ for any $\omega(\sigma, \tau)$. Both actions have the following symmetries: spacetime Poincaré invariance and worldsheet diffeomorphism invariance.

formalism. For the first one, the Polyakov action is extended to a supersymmetric action

$$S = -\frac{T}{2} \int d\sigma d\tau (\partial_a X^\mu \partial^a X_\mu - i\bar{\psi}^\mu \rho^a \partial_a \psi_\mu) \, , \tag{2.19}$$

where $\rho^a (a = 0, 1)$ are Dirac matrices and ψ is a fermion field. The equations of motion for the fermion fields are given by the massless Dirac equation in two dimensions. After applying the canonical quantization one can calculate the spectrum. (It is in part obtained by projecting out some of the bosonic string states.) Now, the superstring critical dimension is $D = 10$. The superstring is stable and the Kaluza-Klein dimensional reduction needs to be applied to get a 4-dimensional theory. Imposing self-consistent backgrounds for strings, the low-energy limit ($\alpha' \to 0$) of string theory is supergravity. Depending on the number of supersymmetries and minimal fermions (and other properties), there are different types of string theories in 10 dimensions. Relevant for the holographic approach is type IIB supergravity, which has two minimal 10-dimensional fermions of the same chirality.

An important concept are D-branes (for a comprehensive discussion see e.g. [17]). These are $(p + 1)$-dimensional endpoints of strings, that act as dynamical walls. They are introduced as follows: In contrast to closed strings, open strings need to have boundary conditions defined on the endpoints. Therefore, there is an additional boundary term in the Polyakov action:

$$\delta S_{P,boundary} = -\frac{1}{2\pi\alpha'} \int d\tau \sqrt{-\gamma} \delta X^\mu \times \partial^\sigma X_\mu |_{\sigma=0}^{\sigma=l} \, . \tag{2.20}$$

In case of Neumann boundary conditions ($\partial^\sigma X_\mu = 0$ at $\sigma = 0, l$) the endpoints move with the speed of light. Dirichlet boundary conditions ($\delta X^\mu = 0$ at $\sigma = 0, l$) imply fixed endpoints. There exist $(p + 1)$ Neumann boundary conditions (in p spatial dimensions plus time) and $(D - p - 1)$ Dirichlet boundary conditions. As a constraint, the string endpoints live on $(p + 1)$-dimensional dynamical (and perhaps different) walls, so-called D- or Dp-branes. One can prove that N coincident D-branes give an U(N) gauge group and that there is a theory of open strings in the adjoint of U(N). The important fact for the holographic principle is, that the low-energy limit of this theory is a SU(N) Yang-Mills theory. Thus, in 4 dimensions, the theory on the world-volume of N $D3$-branes is $\mathcal{N} = 4$ Super Yang-Mills.[3] [4]

2.4 AdS/CFT correspondence

The following sections outline the holographic principle. The AdS/CFT correspondence was originally conjectured by Maldacena in [19]. Gubser, Klebanov and Polyakov worked out de-

---

[3]It is beyond the scope of this thesis to give a introduction to supersymmetric Yang-Mills theory; see e.g. [18] for a detailed discussion.

[4]The quantity $\mathcal{N}$ represents the number of independent supersymmetries of the algebra [18], i.e. the number of noncommutative operators, which generate supersymmetric transformations.

tails in [20]. A precise operator-field correspondence was proposed by Witten in [21]. However, the following discussion is based on [15], which is especially recommendable for an introductory level.

2.4.1 Anti de Sitter space

Anti de Sitter (AdS) space in d dimensions can be defined by an embedding in $(d+1)$ dimensions as the Lorentzian version of a Lobachevski space:

$$ds^2 = -dx_0^2 + \sum_{i=1}^{d-1} dx_i^2 - dx_{d+1}^2 \ , \qquad -x_0^2 + \sum_{i=1}^{d-1} x_i^2 - x_{d+1}^2 = -R^2 \ . \tag{2.21}$$

The AdS space has a SO(2, d-1) invariance.[5] It is possible to write the metric of this space in various coordinates. Global coordinates cover the whole space (in contrast to Poincaré coordinates[6]) with the metric

$$ds_d^2 = R^2(-\cosh^2\rho \ d\tau^2 + d\rho^2 + \sinh^2\rho \ d\vec{\Omega}_{d-2}^2) = \frac{R^2}{\cos^2\theta}(-d\tau^2 + d\theta^2 + \sin^2\theta \ d\vec{\Omega}_{d-2}^2) \tag{2.22}$$

with $d\vec{\Omega}_{d-2}^2$ as the metric on the unit $(d-2)$-dimensional sphere, $\tau \in [0, 2\pi]$ and $\rho \in \mathbb{R}^+$. The last equality is gained by the change $\tan\theta = \sinh\rho$ with $\theta \in [0, 2\pi]$. Using the transformations $r \equiv R\sinh\rho$ and $t \equiv R\tau$, the metric becomes

$$ds_d^2 = -f(r)dt^2 + \frac{1}{f(r)}dr^2 + r^2 d\vec{\Omega}_{d-2}^2 \ , \qquad f(r) = 1 + \frac{r^2}{R^2} \ . \tag{2.23}$$

AdS space can be represented by the Penrose diagram, which is a cylinder obtained by the rotation of the infinite strip between $\theta = 0$ and $\theta = \pi/2$ around the $\theta = 0$ axis. The boundary of AdS_d in global coordinates is $\mathcal{R}_\tau \times S_{d-2}$ with $\mathcal{R}_\tau$ as the infinite vertical line of time and S is a sphere.

Moreover, AdS_n space is a n-dimensional solution of the Einstein equations with the Lagrangian density $\mathcal{L} = \frac{1}{16\pi G_n}(R - 2\Lambda)$. There is a negative cosmological constant (due to the second constant term in $\mathcal{L}$), related to a constant energy-momentum tensor via $T_{\mu\nu} = \Lambda g_{\mu\nu}$. Thus, the field equations are [22]

$$R_{\mu\nu} - \frac{1}{2}g_{\mu\nu}R + \Lambda g_{\mu\nu} = 0 \ . \tag{2.24}$$

AdS space is a maximal symmetric space with constant negative curvature.

---

[5]That group rotates the first d coordinates x_μ by $x'^\mu = \Lambda^\mu{}_\nu x^\nu$.

[6]The metric in Poincaré coordinates is given by $ds^2 = \frac{R^2}{x_0^2}\left(-dt^2 + \sum_{i=1}^{d-2} dx_i^2 + dx_0^2\right)$ with $-\infty < t, x_i < +\infty; 0 < x_0 < +\infty$.

2.4.2 Conformal field theories

Conformal field theories (CFT) are quantum field theories which are invariant under conformal transformations. This involves coordinate transformations that act on flat space in d dimensions $(R^{1,d-1})$ and are defined by $x_\mu \mapsto x'_\mu(x)$ so that

$$dx'_\mu dx'_\mu = [\Omega(x)]^{-2} dx_\mu dx_\mu \ , \tag{2.25}$$

whereby $[\Omega(x)]^{-2}$ is a space dependent scale factor.

In QFT, the procedure of renormalization introduces a renormalization- or energy-scale μ into the theory. The β function characterizes the running of the coupling constant g with the scale:

$$\beta(g) = \mu \frac{dg}{d\mu} \ . \tag{2.26}$$

A scale invariant theory[7] is per definition μ-independent and thus has a zero β function. More generally, a scale invariant theory obeys mostly also a larger conformal invariance. The infinitesimal conformal transformation is

$$x'_\mu = x_\mu + v_\mu(x) \ , \qquad \Omega(x) = 1 - \sigma_\nu(x)$$
$$\Rightarrow \partial_\mu v_\nu + \partial_\nu v_\mu = 2\sigma_\nu \delta_{\mu\nu} \Rightarrow \sigma_\nu = \frac{1}{d} \partial \cdot v \tag{2.27}$$

with the general solution $(d > 2)$

$$v_\mu(x) = a_\mu + \omega_{\mu\nu} x_\nu + \lambda x_\mu + b_\mu x^2 - 2 x_\mu b \cdot x \ . \tag{2.28}$$

The terms $\lambda, a_\mu, b_\mu, \omega_{\mu\nu}$ correspond to scale transformations, translations, special conformal transformations[8] and rotations. In $d > 2$ Minkowski dimensions, the symmetry group of these conformal transformations is SO(2, d). Remarkably, AdS_{d+1} has got the same invariance group. This may be understood as a hint of a relation between a conformal field theory in d-dimensional Minkowski space and a gravitational theory in AdS_{d+1}.

$\mathcal{N} = 4$ Super Yang-Mills theory in 4 dimensions is a representation of the conformal group. It has a SU(N) gauge group and the fields $\{A^a_\mu, \psi^{ai}_\alpha, \phi^a_{[ij]}\}$. This theory possesses quantum scale invariance since the β function is zero.

---

[7]Scale transformations are defined by $x'^\mu = \alpha x^\mu \Rightarrow ds^2 = d\vec{x}'^2 = \alpha^2 d\vec{x}^2$. Thus a scale invariant theory is independent of α.

[8]Special conformal transformations are defined by $x^\mu \mapsto \frac{x^\mu + b^\mu x^2}{1 + 2x^\nu b_\nu + b^2 x^2}$.

2.4.3 The correspondence: Motivation, definition and validity

As already indicated, AdS/CFT correspondence establishes a connection between a d-dimensional CFT and a gravity theory in $(d + 1)$-dimensional AdS space. We regard $d = 4$ with $\mathcal{N} = 4$ supersymmetric Yang-Mills theory with gauge group SU(N) as the CFT and string theory as the gravity theory.

A first step for the motivation of the duality is the equivalence of D-branes and (extremal) p-branes.[9] (The proof was performed by Polchinski in [23].) $\mathcal{N} = 4$ supersymmetric Yang-Mills theory with gauge group SU(N) is the low-energy theory on the worldvolume of N $D3$-branes. On the other side, extremal p-branes are yielded as solutions of supergravity, which itself is the low-energy limit ($\alpha' \to 0$) of string theory.[10] In addition, they also have $\mathcal{N} = 4$ supersymmetry in $d = 4$. Thus, the supergravity solution

$$ds^2 = H^{-1/2}(r)d\vec{x}_\parallel^2 + H^{1/2}(r)(dr^2 + r^2 d\Omega_5^2), \quad H(r) = 1 + \frac{R^4}{r^4}, \ R = 4\pi g_s N\alpha', \ Q = g_s N \quad (2.29)$$

corresponds to N $D3$-branes (which therefore curve space). A p-brane can emit Hawking radiation. Due to the equivalence, this radiation is dual to the collision of two open strings (living on a D-brane) to form a closed string, which can peel of the brane and move away as Hawking radiation.

One can heuristically derive the correspondence from two different points of view:

- On the one hand, we consider the D-branes with the action

$$S = S_{bulk} + S_{brane} + S_{interactions} \ . \quad (2.30)$$

  The first term refers to closed strings living in the bulk of spacetime. They are related to supergravity coupled to the massive modes of the string. The second term refers to open strings living on the $D3$-branes. The last term corresponds to the unitary quantum process, described above. In the low-energy limit ($\alpha' \to 0$), one has $S_{bulk} \to S_{supergravity}$, $S_{brane} \to S_{\mathcal{N}=4SYM}$ and $S_{int} \to 0$. The last relation is valid, because $S_{int} \sim g_s\alpha'$. Thus, (super-)gravity becomes free and there are two decoupled (i.e. non-interacting) systems: Free gravity in the bulk of spacetime and 4-dimensional $\mathcal{N} = 4$ Super Yang-Mills on the $D3$-branes.

- On the other side, we consider p-branes, i.e. supergravity solutions. One can show that there are also two decoupled systems of excitations at low energies. First, gravity

---

[9] p-branes were introduced previously through the p-brane action. However, they can be also regarded as black holes that extend in p spatial dimensions. Extremal p-branes satisfy $M = Q$. Here, M represents the mass and Q the charge.

[10] It is beyond the scope of this thesis to give a introduction to supergravity. However, for a comprehensive discussion see [24, 25]. The latter one is the most complete review of AdS/CFT correspondence.

becomes free at large distances (= low energies or away from the p-brane in the bulk of spacetime). Second, at small distances, there exist low-energy excitations.

Identifying the two systems, we obtain the result, that $\mathcal{N} = 4$ Super Yang-Mills theory with gauge group SU(N) on the $D3$-branes at large N corresponds to the gravity theory at small distances in the D-brane background within the limit $\alpha' \to 0$. Thus, it is necessary to specify this gravity theory:

The supergravity solution (2.29) becomes for $r \to 0$ with $H \approx \frac{R^4}{r^4}$

$$ds^2 \approx \frac{r^2}{R^2}(-dt^2 + d\vec{x}_3^2) + \frac{R^2}{r^2} + R^2 d\Omega_5^2 \tag{2.31}$$

and with the transformation $r/R \equiv R/x_0$

$$ds^2 = R^2 \frac{-dt^2 + d\vec{x}_3^2 + dx_0^2}{x_0^2} + R^2 d\Omega_5^2 \ . \tag{2.32}$$

In fact, equation (2.32) is the metric of $AdS_5 \times S_5$ whereby AdS_5 is in Poincaré coordinates and S_5 is a 5-sphere with radius R. In this space, the gauge theory lives at $r \to \infty$ or $x_0 \to 0$, therefore in the 4-dimensional Minkowski boundary of AdS_5. Remarkably, N is the number of $D3$-branes on the string theory side and the rank of the SU(N) gauge group on the CFT side. The string coupling g_s is related to the Yang-Mills coupling by[11]

$$g_s = g_{YM}^2 \ . \tag{2.33}$$

In summary, AdS/CFT correspondence relates string theory in its supergravity limit in $AdS_5 \times S_5$ with $\mathcal{N} = 4$ supersymmetric Yang-Mills theory with gauge group SU(N) in 4 dimensions at the Minkowski boundary of AdS_5 (in Poincaré coordinates).

As a next step, we consider the limits of validity of the correspondence. One makes the transition from a quantum string to a classical string and then to supergravity. The latter requires $R = \sqrt{\alpha'}(g_s N)^{1/4} \gg l_s$. This is fulfilled if $g_s N \gg 1$ or $g_{YM}^2 N \gg 1$. Since quantum string corrections need to be small, $g_s \to 0$ must hold. Thus, for supergravity, we need the limits: $g_s \to 0$, $N \to \infty$ and $\lambda \equiv g_s N = g_{YM}^2 N$ constant and large ($\gg 1$). On the other side, in the gauge theory, the 't Hooft coupling $\lambda \equiv g_{YM}^2 N$ is small for large N: $\lambda \ll 1$ in contrast to the other approximation. These opposite regimes justify the notion *duality*.

AdS/CFT correspondence is valid in different versions:

- In the strongest form, AdS/CFT correspondence relates string theory in $AdS_5 \times S_5$ to $\mathcal{N} = 4$ Super Yang-Mills with gauge group SU(N) at any $g_s = g_{YM}^2$ and N. This regime

---

[11] As an example, two open string splitting interactions, governed by g_{YM}, are dual to one closed string splitting interaction, governed by g_s.

is believed to be true.

- A strong version is valid at any finite $g_s N$ under the constraint $N \to \infty$ and $g_s \to 0$. This corresponds to the 't Hooft limit of a QFT: $N \to \infty$, $g_{YM} \to 0$, $N g_{YM}^2 = const$.

- The weakest version of AdS/CFT correspondence relates supergravity in $AdS_5 \times S_5$ with $\mathcal{N} = 4$ Super Yang-Mills with gauge group SU(N) and $g_{YM}^2 = g_s$ at $g_s \to 0$, $N \to \infty$ and $\lambda = g_s N$ fixed and large ($\gg 1$).

Finally, it should be stated that the holographic principle can also relate global AdS_5 space to $\mathcal{N} = 4, d = 4$ Super Yang-Mills theory. In this case, string theory in global $\text{AdS}_5 \times S_5$ space corresponds to a CFT on the $\mathcal{R}_\tau \times S_3$ space, which represent the boundary of global AdS_5.

2.4.4 Operator-field duality and Witten prescription

The Witten prescription outlines a precise correspondence between observables and correlators of the CFT and those of supergravity. In fact, this section shall give just a very short and basic idea of this duality. See [15, 25] for detailed explanations.

Let us consider the Euclidean version of AdS_5. Then, the operator-field duality states that an scalar operator $\mathcal{O}$ in $\mathcal{N} = 4$ Super Yang-Mills of scaling dimension Δ is related to a field ϕ of mass m in $AdS_5 \times S_5$ supergravity with the relation

$$\Delta = \frac{d}{2} + \sqrt{\frac{d^2}{4} + m^2 R^2} \ . \tag{2.34}$$

Applying the Kaluza-Klein procedure of compactification reduces the supergravity fields on S_5.[12] Furthermore, let ϕ_0 be the value of a massless field on the boundary of AdS_5. The interpretation is that ϕ_0 is a source for $\mathcal{O}$. Then, $\mathcal{O}$ must be a composite operator. On the field theory side, one can calculate the partition function with sources for $\mathcal{O}$. This is a generating functional of correlation functions of the operator and allows the calculation of expectation values (in Euclidean space):

$$Z_\mathcal{O}[\phi_0] = \int \mathcal{D}\phi \ e^{-S_{\mathcal{N}=4SYM} + \int d^4 x \mathcal{O}(x)\phi_0(x)} \tag{2.35}$$

$$\Rightarrow \langle \mathcal{O}(x_1) \dots \mathcal{O}(x_n) \rangle = \frac{\delta^n}{\delta\phi_0(x_1) \dots \delta\phi_0(x_n)} Z_\mathcal{O}[\phi_0] \Big|_{\phi_0 = 0} \ . \tag{2.36}$$

In AdS_5, $Z_\mathcal{O}[\phi_0]$ should be a partition function of classical supergravity for the field ϕ with source ϕ_0 on its boundary, since we do not expect quantum corrections in the limit $g_s \to 0$, $\alpha' \to 0$, $g_s N \gg 1$. Thus we have

$$Z[\phi_0] = e^{-S_{supergravity}[\phi[\phi_0]]} \ . \tag{2.37}$$

---

[12]This procedure allows also the following duality: Gravity on AdS_5 is dual to a CFT in 4 dimensions.

Finally, Wittens prescription for the correlation functions of massless fields becomes

$$Z_{\mathcal{O}}[\phi_0]_{CFT} = \int \mathcal{D}\phi \; e^{-S + \int d^4 x \mathcal{O}(x)\phi_0(x)} = Z_{classical}[\phi_0]_{AdS} = e^{-S_{supergravity}[\phi[\phi_0]]} \; . \qquad (2.38)$$

A more general form states [16]

$$Z_{string}(\phi_0) = \int_{\phi_0} \mathcal{D}\phi \; e^{-S_{string}} = \left\langle \exp \int_{S^d} \phi_0 \mathcal{O} \right\rangle_{CFT} . \qquad (2.39)$$

3 Evaluation of the lattice data results

Lattice gauge theory is a formulation of quantum field theory with gauge symmetries on a space-time lattice [26]. It has become a standard method for non-perturbative gauge theory calculations, particular for QCD. The main idea is to evaluate the partition function stochastically on a finite number of Euclidean spacetime points. To obtain physical results, the continuum limit needs to be taken ($a \to 0$ or $N_\tau \to \infty$).[13] The main quantity is the interaction measure (or trace anomaly) that is determined directly from the partition function. Other thermodynamic quantities are calculated out of it.

Essentially, our analyses are based on results of two collaborations that perform lattice QCD studies: The *Wuppertal-Budapest* (WuB) and the *hotQCD* collaborations. This chapter aims to analyze these data since the holographic model is fitted to the QCD lattice results. The WuB data are taken from [11] and the hotQCD data originated from [27]. Both collaborations calculate the QCD equation of state at zero baryon chemical potential ($\mu_B = 0$) with physical quark masses.

Figure 3.1 shows the entropy density s, the speed of sound c_s^2, the pressure p and the interaction measure I in dependence of the temperature T. To obtain dimensionless values, the quantities p and I are usually scaled with T^4, while s uses a scaling with T^3. The graphs contain two different data sets from the hotQCD collaboration, referred to as *HISQ/tree* and *stout*. These are based on different lattice actions. As one can see, the WuB and the stout data agree very well with respect to s, c_s^2 and p, although there are differences in the interaction measure. Note that also the uncertainties are of the same order of magnitude. The last graph in figure 3.1 illustrates the interaction measure in dependence of different discretizations of the hotQCD data. As mentioned, these data vary from those of the WuB collaboration. However, the differences are much smaller in contrast to older data (denoted as *asqtad* and *p4* in the graph) that result in much higher T_c values. Since the WuB lattice data are calculated in a larger temperature range (110-510 MeV) and agree with the hotQCD results (130-400 MeV), we will just consider these data for the holographic model.

The arrows in the plots denote the Stefan-Boltzmann limits that represent an ideal gas of

---

[13]The QFT is discretized on $N_s^3 \times N_\tau$ lattice points and the temperature is given by $T = 1/(aN_\tau)$ whereby a is the discretization interval.
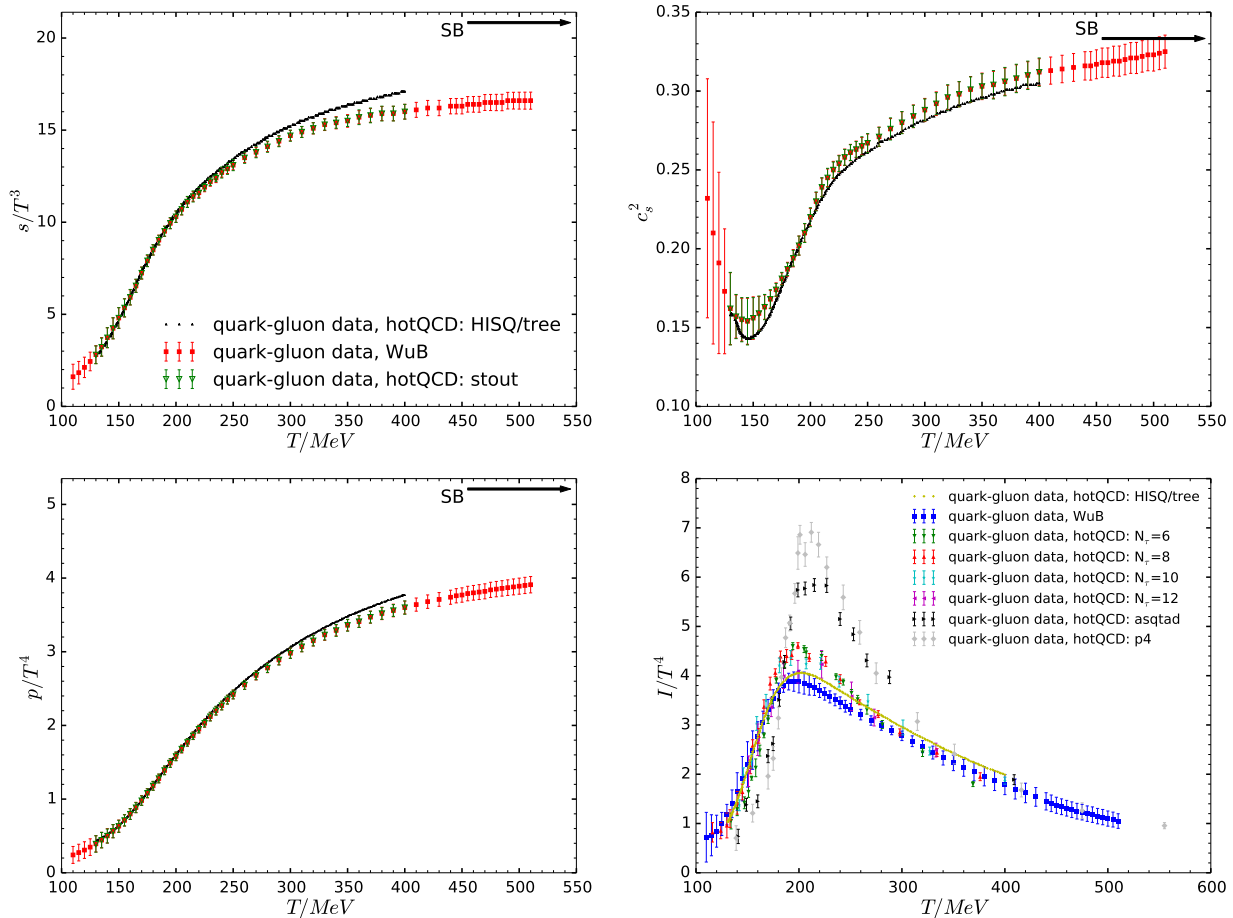
Figure 3.1: Comparison of the lattice QCD results from the WuB collaboration [11] and the hotQCD collaboration [27] in dependence of the absolute temperature T. The arrow denotes the Stefan-Boltzmann limit.

massless, free, relativistic quarks and gluons. The values are given by

$$\frac{p_{SB}}{T^4} = \frac{\pi^2}{90} g_{QGP} \ , \qquad \epsilon_{SB} = 3 p_{SB} \ , \qquad s_{SB} = \frac{4 p_{SB}}{T} \ , \qquad c^2_{s,SB} = \frac{dp_{SB}}{d\epsilon_{SB}} = \frac{1}{3} \ . \qquad (3.1)$$

g_{QGP} is the number of degrees of freedom and it is determined by $g_{QGP} = g_g + \frac{7}{8} g_q$ whereby g_g and g_q are the bosonic (gluons) and fermionic (quarks) degrees of freedom.[14] They are calculated as follows: $g_g = 2_{spin} \cdot (N_c^2 - 1) = 16$, $g_q = 2_{spin} \cdot 2_{q\bar{q}} \cdot N_c \cdot N_f = 36$ ($N_f = 3$). As one can see in figure 3.1, the entropy density and pressure are far away from an ideal gas. Even for the highest temperatures, the quantities are still almost 20 % below the Stefan-Boltzmann limits. The interaction measure for an ideal gas vanishes since I is defined as $I \equiv \epsilon - 3p$. Thus, the trace anomaly is a useful measure for the deviation of the QGP from ideal gas behavior.

In contrast to pure SU(N) Yang-Mills theory, which exhibits a first-order deconfinement phase

---

[14]The factor 7/8 takes into account the different quantum statistics and is obtained by the integration over a fermionic distribution.

transition for $N \geq 3$, the transition of the QGP from a phase of colored degrees of freedom to a phase dominated by hadrons occurs as a crossover. Thus, there is no real phase transition. One of the most important parameters is the transition temperature T_c, which introduces an absolute scale. The WuB collaboration obtains the range $T_c \approx 150 - 170 \, \text{MeV}$ for the crossover [11, 12]. There is no unique transition temperature since different observables lead to different T_c definitions. Particularly for the interaction measure and using a $N_t = 8$ lattice, the result is

$$\text{WuB:} \qquad T_c = 154 \pm 7 \, \text{MeV} \, , \qquad\qquad (3.2)$$

whereby T_c is defined as the inflection point of the curve $I/T^4(T)$. However, different pseudocritical T_c values for various quantities do not indicate that a phase transition happens at different temperatures. These variations are just a characteristic of the crossover [12]. For instance, for the entropy $s/T^3(T)$, a characteristic point is the inflection point. A calculation of this point with two different methods (using smoothed splines and a high-order polynomial) yielded $T_c \approx 160 \, \text{MeV}$. These different T_c ranges will be considered in subsequent fit procedures. The hotQCD collaboration calculates T_c by two different methods (based on a continuum extrapolation using two actions with physical quark masses and on the peak position of the chiral susceptibility). The values are:

$$\text{hotQCD:} \qquad \text{method 1: } T_c = 154 \pm 9 \, \text{MeV}, \qquad \text{method 2: } T_c = 155 \pm 9 \, \text{MeV}. \qquad (3.3)$$

All estimates are in very good agreement within the error margins.

An interesting aspect are the differences between the equation of state of the pure gluon and the quark-gluon plasma. Figure 3.2 shows both lattice data. The entropy density and pressure of the QGP attain higher values. The reason is the number of degrees of freedom: The approximate ratio is 25:16. The number 16 results from 8 gluon colors and a factor of 2 for the polarisation. The factor 25 is the product $2 \cdot 2 \cdot 3 \cdot 2.5$ with respect to antiparticles, spin, color and quark flavors (u, d, c weighted). The different Stefan-Boltzmann limits are also a measure of the ratio of the degrees of freedom. Note that the pure gluon plasma is just $13\,\%$ below the SB limit of the entropy density at $T = 3.5 \, T_c$ in contrast to the QGP. Remarkably, the speed of sound of the QGP is much less smooth in comparison to the gluon data. Moreover, c_s^2 has no zero in case of the QGP and the values increase for temperatures below T_c. This behavior is indicating a crossover in contrast to the pure gluon data, where a first-order phase transition occurs. In addition, figure 3.3 (right side) shows differences between the interaction measure. The gluon data are scaled so that the maximum point and maximum value match. This representation shows that the main difference occurs for higher T: After a steep slope, the pure gluon lattice data reach faster small values. The left side of figure 3.3 shows a fit function for the interaction measure, that is proposed by the WuB collaboration. However, this is only
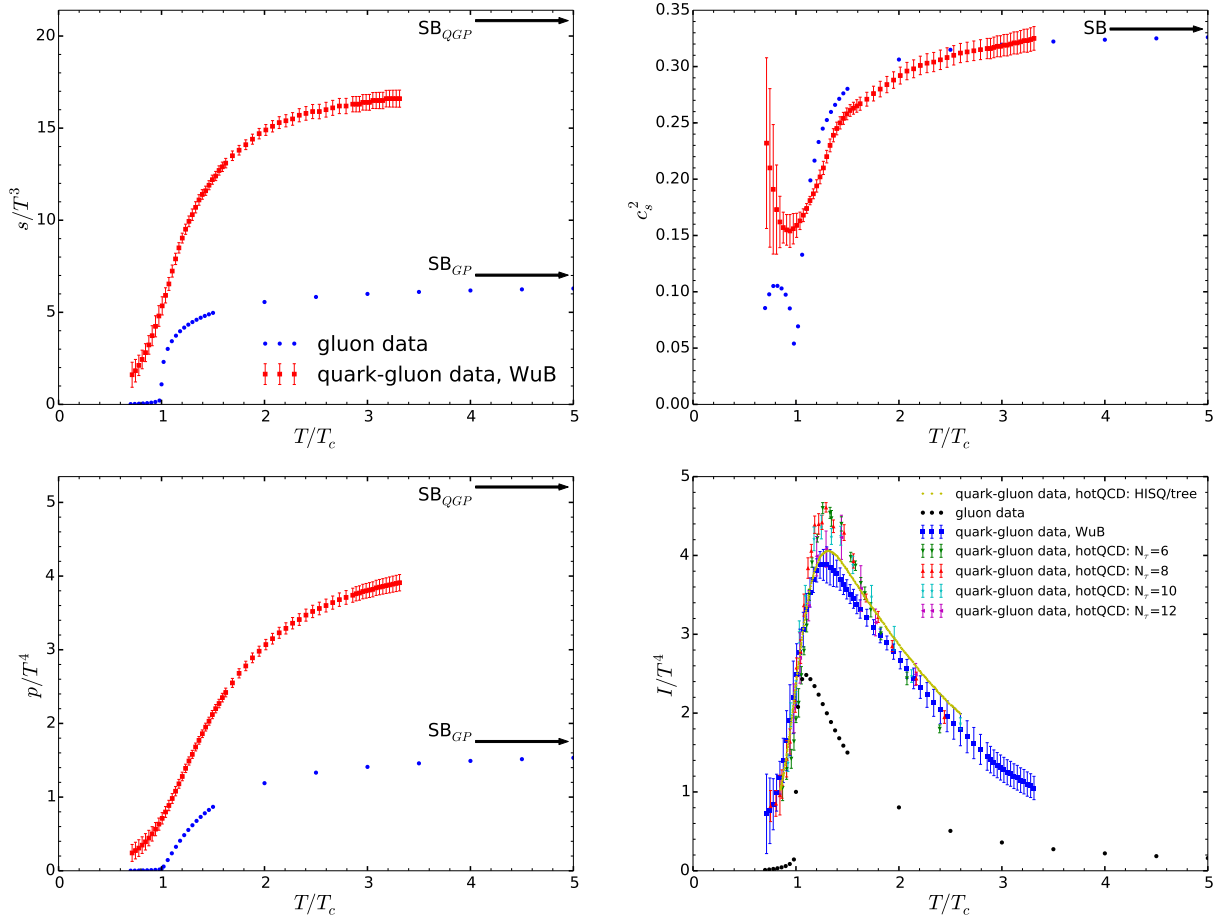
Figure 3.2: Comparison of the lattice QCD results from the WuB collaboration [11] and and previous pure gluon lattice data [28] in dependence of the scaled temperature T/T_c. The interaction measure contains also the new hotQCD results [27]. The arrows denote the Stefan-Boltzmann limits for the QGP and pure gluon plasma (GP).

a numerical fit function and has no deeper justification. Therefore it is not considered further.

For a deeper understanding, the pressure, entropy density and speed of sound were recalculated with the interaction measure as input. The quantities are following from the relations [29]

$$I \equiv \epsilon - 3p = T^5 \frac{\partial}{\partial T}(p/T^4) \Rightarrow \frac{p}{T^4} = \int dT \frac{I}{T^5} + const \ , \tag{3.4}$$

$$\frac{s}{T^3} = \frac{\epsilon + p}{T^4} = \frac{I + 4p}{T^4} \ , \tag{3.5}$$

$$\epsilon = I + 3p \ , \tag{3.6}$$

$$c_s^2 = \frac{dp}{d\epsilon} \Leftrightarrow c_s^2 = \frac{d \ln T}{d \ln s} \ . \tag{3.7}$$

Thus, the scaled pressure is obtained through integration of the interaction measure. The appropriate integration constant comes from a Hadron Resonance Gas model. Since this value is unknown to us, the first lattice point from the WuB collaboration was taken. The scaled
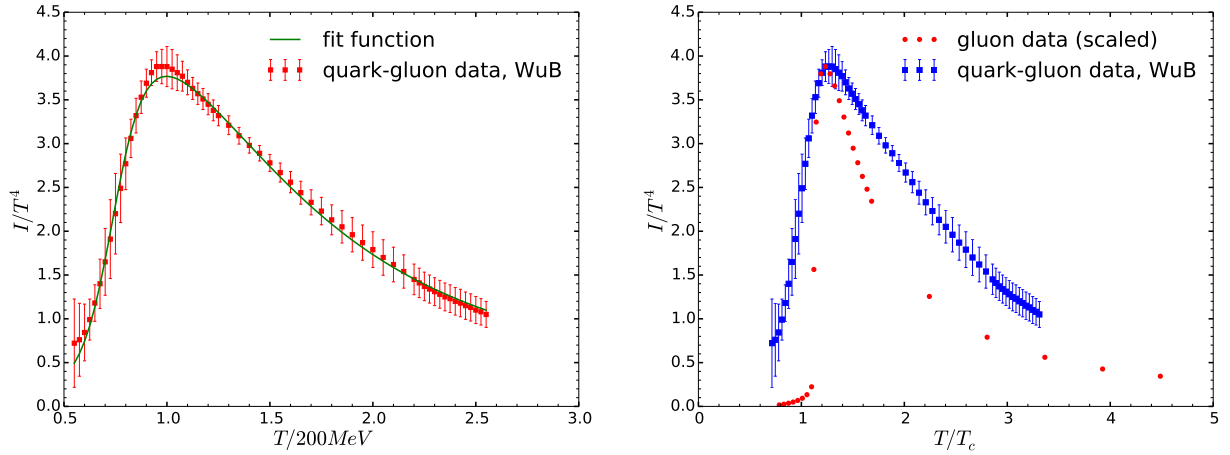
Figure 3.3: Representation of the interaction measure and the suggested fit function from WuB collaboration [11] (left side). Scaled interaction measure of the gluon [28] and quark-gluon [11] lattice data (right side).

entropy density is a linear combination of I/T^4 and p/T^4 (relation (3.5)). Figure 3.4 shows the results of the calculation.
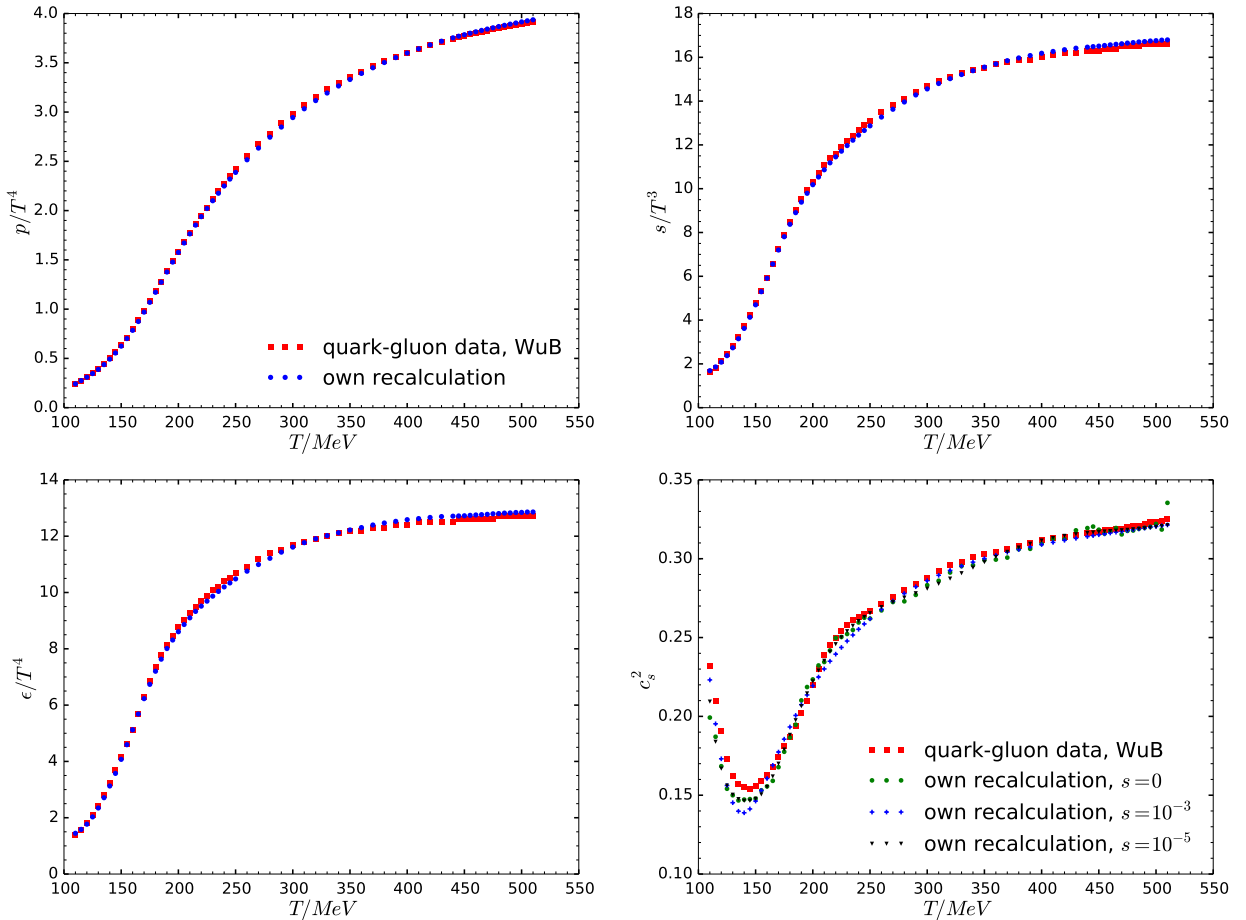

Figure 3.4: Comparison of the lattice QCD results [11] (WuB collaboration, red squares) with the own recalculation (blue dots) with the interaction measure from [11] as input.

This recalculation was numerically performed with B-splines of order 5 that interpolate between lattice points. For values below $400 \, \mathrm{MeV}$, the recalculation underestimates the pressure and entropy density. Moreover, the original lattice data do not fulfill relation (3.5) for each data point: There is a maximal discrepancy of 0.21 for $T = 210 \, \mathrm{MeV}$. The last plot in figure 3.4 shows the speed of sound. Using B-spline interpolations (green dots), the numerical result is less smooth than the lattice data points. This behavior is independent of the used formula in (3.7). Thus, we applied a smoothing condition, such that $\sum [y(T) - g(T)]^2 \leq s$, where $y(T)$ are the lattice points and $g(T)$ is the smoothed interpolation. The plot shows the results for two different smoothing factors s (blue and black marks). In fact, the lattice data points cannot be reproduced exactly. This implies that smoothing effects have been applied by the collaboration, which are not described in detail. That is why the lattice data points should always be considered only in the context of their error bars.

4 Holographic models

In the following, the AdS_5/CFT_4 correspondence is used to calculate the equation of state of the QGP. In fact, the holographic principle cannot be directly applied to QCD or Yang-Mills theory (see [10] for more detailed discussions). One reason is the gauge theory limit $N \to \infty$ that is needed to perform calculations in the non-quantum gravity sector, whereas in QCD one has $N = N_c = 3$. Furthermore, the gravity approximation is strictly valid in the limit of infinite 't Hooft coupling $\lambda \to \infty$, while one is interested in large but finite coupling calculations. However, the coupling in the temperature range of the lattice data and transition temperatures seems to be a good approximation. The dual to the gravity theory is $\mathcal{N} = 4$ SYM theory as a CFT. A characteristic of this is a vanishing β function. In contrast, QCD has a non-trivial β function and besides, it is not a supersymmetric theory. Despite all these difficulties, AdS/CFT correspondence has been successfully applied to QCD, mainly for the description of pure gluon lattice data [30,31]. In this case, one speaks of AdS/QCD correspondence. The following two sections consider both bottom-up models.[15] These models make the assumption that a gravity dual exists and is given by non-supersymmetric Einstein's GTR. The emphasis lies on the reproduction of the QCD properties. Five-dimensional Einstein gravity is coupled to a scalar field ϕ with a non-trivial potential $V(\phi)$. The SYM theory is conformally invariant, whereas in QCD conformal invariance is broken due to quantum fluctuations. The basic principle of the holographic models is the translation thereof into the deformation of the conformally invariant AdS space due to a non trivial scalar field potential [10].

The numerical setup for the following results is based on the work of Yaresko in [10].

4.1 The Kiritsis model

Kiritsis *et al.* developed a holographic model in [32–34] (denoted as *Kiritsis model* in the following). The comparison with gluon lattice data was performed in [31]. The holographic dual of large-N_c Yang-Mills theory is based on a 5D Einstein dilaton model with the action

$$S_5 = -M_p^3 N_c^2 \int d^5x \sqrt{g} \left[R - \frac{4}{3}(\partial\Phi)^2 + V(\Phi) \right] + 2M_p^3 N_c^2 \int_{\partial M} d^4x \sqrt{h} K \ . \qquad (4.1)$$

---

[15]On the other side, one has more rigorous top-down models; see e.g. [10] for explanations.

Here, M_p is the 5D Planck scale and the second term is the Gibbons-Hawking term with K as the extrinsic curvature of the boundary and h is the determinant of the induced metric on it.[16] The effective 5D Newton constant is $G_5 = 1/(16\pi M_p^3 N_c^2)$. One defines usually $\lambda \equiv e^\Phi$. Einstein's field equations are (see [34] for calculations)

$$G_{\mu\nu} - \frac{4}{3}\left[\partial_\mu\Phi\partial_\nu\Phi - \frac{1}{2}(\partial\Phi)^2 g_{\mu\nu}\right] - \frac{1}{2}g_{\mu\nu}V = 0 , \qquad \Box_5 + \frac{\partial V}{\partial\Phi} = 0 . \tag{4.2}$$

With the ansatz $ds^2 = e^{2A}(-f dt^2 + dx^2) + \frac{du^2}{f}$ the field equations become:

$$
\begin{aligned}
12A'^2 + 3A'g' - \frac{4}{3}\Phi'^2 - e^{-g}V = 0 , & \qquad A'' + \frac{4}{9}\Phi'^2 = 0 , \\
g' + \frac{g''}{g'} + 4A' = 0 , \qquad \Phi'' + 4A'\Phi' + g'\Phi' + \frac{3}{8}e^{-g}\frac{dV}{d\Phi} = 0 .
\end{aligned}
\tag{4.3}
$$

A prime denotes a derivative w.r.t. u and f and b are defined as $f = e^g$, $b = e^A$. This is usually called the *domain wall frame* and the parametrization of the metric yields $dr = e^{-A}du$ with r as the radial (conformal) coordinate. It is convenient to use scalar variables $X \equiv \Phi'/3A'$ and $Y \equiv f'/4fA'$ for numerical analysis. Thus, one transforms the field equations into a coupled system of two first-order differential equations. Thermodynamic observables are entirely encoded in this system. For a given potential $V(\lambda)$ the equations for X and Y are:

$$\frac{dX}{d\lambda} = -\frac{4}{3\lambda}(1 - X^2 + Y) \cdot \left(1 + \frac{3}{8X}\frac{\lambda d\log V}{d\lambda}\right) , \tag{4.4}$$

$$\frac{dY}{d\lambda} = -\frac{4}{3\lambda}(1 - X^2 + Y)\frac{Y}{X} . \tag{4.5}$$

For the numerical calculations we substituted $Z \equiv \ln Y \Leftrightarrow Y = e^Z$ in equation (4.5). The equations are numerically integrated[17] from a boundary $\lambda_0 = 0.005 \ll 1$ to the horizon λ_h with the following two initial conditions that arise from the requirement for finiteness of $dX/d\lambda$ and $dY/d\lambda$ at the horizon [31]

$$X_h \equiv X(\lambda_h) = -\frac{3\lambda_h \frac{dV}{d\lambda}(\lambda_h)}{8V(\lambda_h)}, \qquad Y_h \equiv Y(\lambda_h) = \frac{9\lambda_h \frac{dV}{d\lambda}(\lambda_h)}{32V\ln\frac{\lambda_h}{\lambda}} = -\frac{3X_h}{4\ln\frac{\lambda_h}{\lambda}} . \tag{4.6}$$

Kiritsis *et al.* use the following ansatz for the potential

$$V(\lambda) = \frac{12}{L^2}\left\{1 + V_0\lambda + V_1\lambda^{4/3}\left[\ln(1 + V_2\lambda^{4/3} + V_3\lambda^2)\right]^P\right\} . \tag{4.7}$$

---

[16]The signature $(-+++)$ is used.

[17]The entire numerical calculations are performed in python using scipy. The integration routine *odeint* is used for solving the differential equations and B-splines are used to interpolate the solutions and to calculate the thermodynamic quantities.

The parameters V_1 and V_3 are free and fitted (see below) whereas $P = 1/2$ is fixed in the original setting. The other parameters are determined by some normalization and UV expansion considerations [31] and are given by

$$V_0 = \frac{8}{9}b_0 \; , \qquad V_2 = b_0^4 \left(\frac{23 + 36b_1/b_0^2}{81V_1} \right)^2 \; , \qquad b_0 = \frac{22}{3(4\pi)^2} \; , \qquad \frac{b_1}{b_0^2} = \frac{51}{121} \; . \tag{4.8}$$

f is called *black hole* or *blackness function* since it defines a black hole at the horizon. To calculate the equation of state, one makes use of the black hole thermodynamics: Hawking [35] and Bekenstein [36] postulated that black holes can be associated with a temperature and an entropy (density), given by

$$T_H = \frac{\varkappa}{2\pi} \bigg|_h \; , \qquad s_{BH} = \frac{A_h}{4G_5 V_h} \tag{4.9}$$

with A_h as the surface of the black hole horizon, $\varkappa$ as the surface gravity and V_h is the horizon volume. In the Kiritsis model, the temperature and entropy then follow from $T = -\frac{\dot{f}(r_h)}{4\pi}$, $S = 4\pi (M_p^3 N_c^2 V_3) b^3(r_h)$, where a dot denotes a derivative w.r.t. r. Alternatively, the equation of state is given by[18]

$$TL = \frac{1}{\pi} \exp \left\{ Z_0 + A_0 - \int_{\lambda_0}^{\lambda_h} d\lambda \frac{1}{X\lambda} \right\} \; , \qquad \frac{s}{T^3} = \frac{\pi^3}{4G_5} \left(\frac{12}{V} \right) \exp \left\{ -4 \int_{\lambda_0}^{\lambda_h} d\lambda \frac{X}{\lambda} \right\} \; . \tag{4.10}$$

In general, A can be regarded as a scale factor and A_0 is calculated as $A_0 = \left| \int_{\lambda_0}^{\lambda_{h,0}} d\lambda \frac{1}{3X\lambda} \right|$ (rounded) with $\lambda_{h,0} = 0.05$. Z_0 is defined as $Z_0 = Z(\lambda_0)$. From (4.10), s is calculated with $s = \frac{s}{T^3}(TL)^3$.

An important point is the definition of the transition temperature T_c. This must be understood in the sense of an ad hoc definition to set a scale for the fit procedure. In this case, T_c is defined as the minimum of the curve $T(\lambda_h)$. If it does not exist, T_c is defined as the inflection point of $\frac{s}{T^3}(T)$.

The other thermodynamic quantities are calculated with the following relations

$$c_s^2 = \frac{s}{T} \left(\frac{dT}{ds} \right) = \frac{d\ln T}{d\ln s}, \qquad p(T) = p_0 + \int_{T_c}^{T} s(T) dT, \qquad \epsilon = sT - p, \qquad I = \epsilon - 3p, \tag{4.11}$$

whereby $p_0 = p(T_c)$ is taken from the lattice data [11].

For the fit procedure, the WuB lattice data were used with the definition $T_c = 155 \, \text{MeV}$[19] and the thermodynamic quantities in the holographic model were calculated in dependence of the

---

[18]by using eqn. (H.67) and under consideration of eqn. (7.38), both in [34].
[19]In the last chapter the value 154 MeV was given. However, for 155 MeV a tabulated data point exists and the hotQCD group obtained also 155 MeV for T_c with one method. Furthermore, the uncertainty is much larger.

scaled temperature T/T_c. Different types of fit procedures were considered:

1. fit of V_1 and V_3 to $c_s^2(T/T_c)$ and afterwards fit of G_5 to $s/T^3(T/T_c)$,

2. fit of V_1, V_3 and G_5 to $s/T^3(T/T_c)$.

A fit to the interaction measure was also tested but did not yield better results. To evaluate the goodness of the fit, the quantities were interpolated as functions of T/T_c using B-splines and a χ^2-function was defined in the following way:

$$\chi^2 = \frac{1}{N-p-1} \sum_{i=1}^{N} \left[\frac{q_h(T_i/T_c) - q_L(T_i/T_c)}{\sigma_{i,L}} \right]^2 . \qquad (4.12)$$

Here q_h is the fitted thermodynamic quantity in the holographic model and q_L the corresponding value from the lattice data. $\sigma_{i,L}$ stands for the error of a lattice point, N is the number of fitted lattice points and p is the number of fitted parameters. The normalization factor is the inverse of the number of degrees of freedom and allows the interpretation as a reduced chi-square statistic [37]. A value in the order of 1 represents a good fit. For the fit procedure itself the simplex method of Nelder and Mead was used.[20] Tables 4.1 and 4.2 summarize the fit results. The implementation of the fit procedures revealed a strong dependence on the initial values and scale settings. Despite numerous investigated initial value ranges and scales, no convergence was found, i.e. fit 1 and 2 do not yield the same results. However, as one can see from the table, fit 2 to the entropy density yields the best results.

Figure 4.1 shows the equation of state of the QGP from fit 2 and further quantities (blue lines). Since we want to describe the deconfinement phase, the holographic equation of state is calculated for temperatures $T/T_c > 1$. As the first plot shows, the entropy density s/T^3 underestimates the lattice data very strongly for the temperature range $T/T_C \gtrsim 1$ and thus the model does not describe the curve shape of the lattice data. Moreover, the speed of sound is badly described, since it assumes the value $c_s^2 = 0$ for $T = T_c$. The curve of the Kiritsis model is smooth in contrast to the lattice results. This is reflected in the fact, that the model overestimates the lattice points for temperatures $T/T_c \approx 1.75$. The high temperature behavior of the model seems to be constant, whereas the data points probably do not exhibit this tendency. The pressure is described very well, whereby one must remember that $p(T_c)$ is taken from the lattice results. The interaction measure overestimates the peak and does not describe the low as well as the high temperature range.

The reason for these problems seems to be the fact, that the Kiritsis model is adjusted to yield a first-order phase transition as needed to describe the pure gluon plasma. In his publications, the author discusses different sizes of black holes and energy ranges. He calculates different

---

[20]In fact $(-\chi^2)$ was maximized. Other methods like the L-BFGS-B algorithm, a downhill simplex algorithm, Powell's method, a nonlinear conjugate gradient algorithm and others did not yield good results or were impractical.

Table 4.1: Parameter values of the different fit procedures.

Fit	Fit type	Fit quantity	V_1	V_3	G_5	P
1	$P = 1/2$ fixed	c_s^2	6.5438	162.2250	0.3466	0.5
2		s/T^3	5.2177	150.0827	0.3745	0.5
3	$P < 0$ fitted	s/T^3	5.0852	150.1697	0.2106	-0.0614

Table 4.2: Parameter values of the different fit procedures.

Fit	$\chi^2_{c_s^2}$	χ^2_{s/T^3}	T_c-type
1	9.5987	1.8606	minimum
2	9.8178	1.2932	minimum
3	30.0723	37.6726	inflection
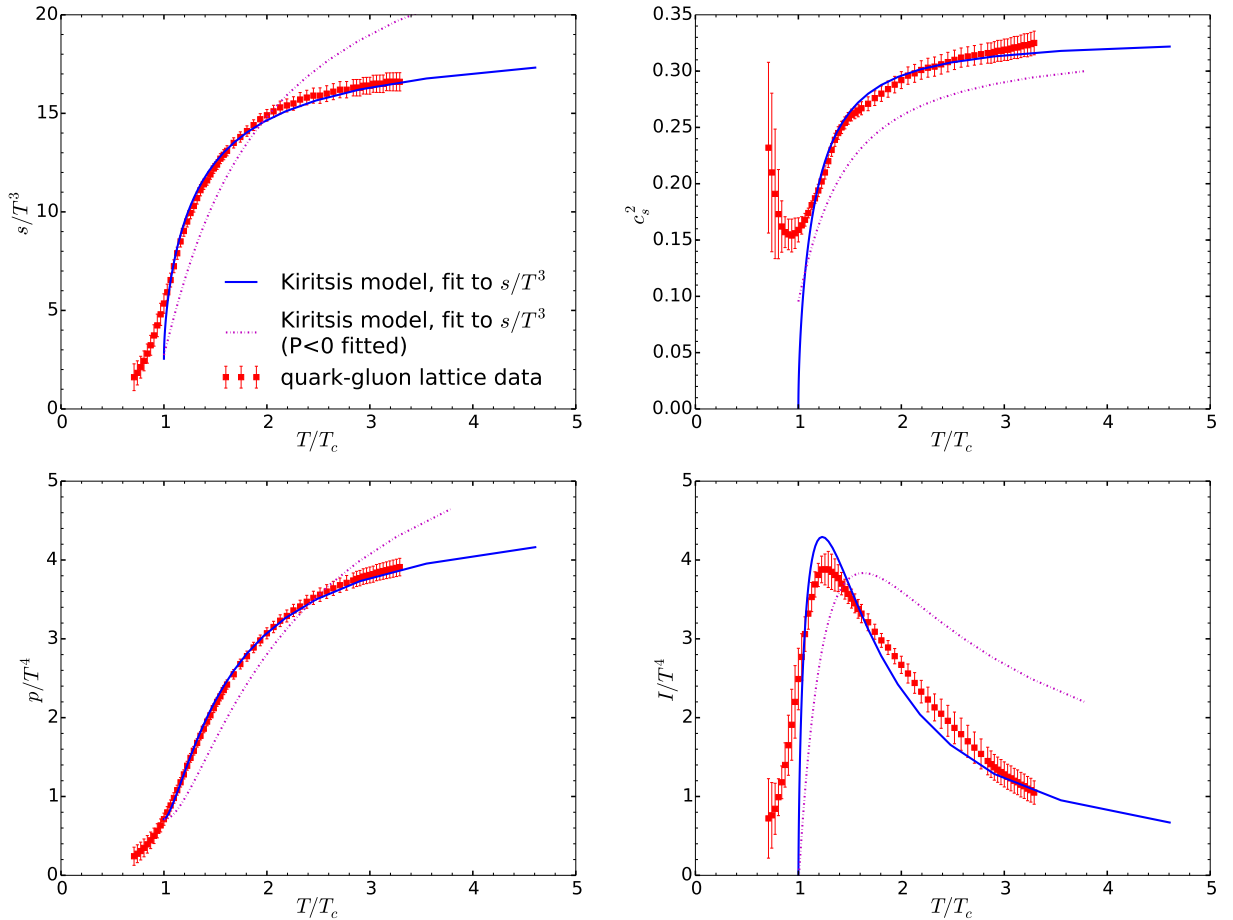
Figure 4.1: Equation of state and thermodynamic quantities of the QGP. The Kiritsis model is fitted to the lattice QCD data [11].

power-law expansions of the potential $V(\lambda)$ for small and large λ (that correspond to the UV and IR region) and sets $P = 1/2$ to reproduce confinement and a linear glueball spectrum (see [34]). To avoid this constraint, we tested, whether $P < 0$ as a free parameter allows a better description of the equation of state. Fit 3 in table 4.1 and 4.2 shows the fit result. The dashed curves in figure 4.1 correspond to this fit. As one can see, this setting describes the equation of state even much worse and there is no match with the lattice data at all.

4.2 The Gubser model

The so-called *Gubser model* was developed by Gubser *et al.* in [30, 38]. It is based on the action

$$S = \frac{1}{16\pi G_5} \int d^5x \sqrt{-g} \left(R - \frac{1}{2}\partial_\mu \phi \partial^\mu \phi - V(\phi) \right) \tag{4.13}$$

with the metric $ds^2 = e^{2A}(-fdt^2 + d\vec{x}^2 + \frac{dz^2}{f}) = e^{2A}(-fdt^2 + d\vec{x}^2) + L^2 e^{2B}\frac{d\phi^2}{f}$. The equality follows from the transformation $dz^2 = \frac{1}{L^2}\frac{dz^2}{d\phi^2}L^2 d\phi^2$ and the definition $e^{2B} \equiv e^{2A}\frac{dz^2}{L^2 d\phi^2}$. The field equations and the ϕ equation of motion take the form [10, 30]

$$A'' - A'B' + \frac{1}{6} = 0 \ , \qquad\qquad f'' + f'(4A' - B') = 0 \ ,$$

$$6A'f' + f(24A'^2 - 1) + 2e^{2B}L^2 V = 0 \ , \qquad 4A' - B' + \frac{f'}{f} - \frac{e^{2B}}{f}L^2 V' = 0 \ , \tag{4.14}$$

where a prime denotes $d/d\phi$.[21] With the definition of two scalar variables $X \equiv \frac{1}{4A'}, Y \equiv \frac{g'}{4A'}$ (whereby g is defined as $g \equiv \ln f$) one can transform the system into

$$X' = -\left(1 + Y - \frac{2}{3}X^2\right)\left(1 + \frac{3V'}{4XV}\right) \ , \tag{4.15}$$

$$Y' = -\left(1 + Y - \frac{2}{3}X^2\right)\frac{Y}{X} \ . \tag{4.16}$$

As in the Kiritsis model, the quantity $Z \equiv \ln Y$ was defined for the numerical calculation. The differential equations are integrated from the horizon ϕ_h to $\phi_0 = 0.001$ with the initial conditions

$$X_h \equiv X(\phi_h) = -\frac{3V'}{4V}(\phi_h) \ , \qquad Y_h \equiv Y(\phi_h) = \frac{X_h}{\phi - \phi_h} \ , \tag{4.17}$$

where $\phi = 0.9999\phi_h$ is set. The ansatz for the potential is [30]

$$V(\phi) = \frac{1}{L^2}\left[-12\cosh(\gamma\phi) + b\phi^2\right] \ , \tag{4.18}$$

---

[21]See appendix A for more detailed explanations.

where the relation $\Delta(\Delta - 4) = M^2 L^2 = 2b - 12\gamma^2$ holds. Here, Δ is the dimension of the gauge theory operator dual to ϕ and M is the mass of the field. The equation of state follows from the relations

$$s = \frac{e^{3A}}{4G_5}\bigg|_{\phi_h}, \qquad TL = -\frac{f'}{4\pi}e^{A-B}\bigg|_{\phi_h} \tag{4.19}$$

and to be more specific:

$$A_h \equiv A(\phi_h) = \int_{\phi_0}^{\phi_h}\left(\frac{1}{4X} - \frac{1}{\phi(\Delta - 4)}\right) + \frac{\ln\phi_h}{\Delta - 4}, \qquad TL = \frac{1}{\pi}e^{Z_0 + A_{UV}(\phi_0,\Delta) - 3a_h} \tag{4.20}$$

$$a_h = A_h - A_{UV}(\phi_0, \Delta), \qquad A_{UV}(\phi, \Delta) = \frac{\ln\phi}{\Delta - 4}. \tag{4.21}$$

The first term in A_h is the inversion of the X-definition and the other terms take into account the boundary asymptotics.

The definition of T_c, the calculation of the other thermodynamic quantities and the fit procedure are performed in the same way as for the Kiritsis model. The results are presented in table 4.3 and figure 4.2 shows the equation of state for $T_{c,lattice} = 155\,\text{MeV}$.

First, one can notice that the χ^2 values are smaller than for the Kiritsis model. In fact, fits to the squared speed of sound yielded the best results. Two ranges of the parameter Δ were found, that allow a good description of the equation of state (denoted as fit 1 and 2). Fit 1 allows a very good description of the (scaled) entropy density. In contrast to fit 2, fit 1 is nearly constant for high temperatures ($T/T_c \gtrsim 3.0$). Since no lattice results for higher temperatures are available, one cannot determine which fit is better in this range. Both fit results are within the uncertainties of the lattice results. The plot of c_s^2 reveals that the lattice points are underestimated in the range $1.3 < T/T_c < 1.6$. In particular in this range, fit 2 is slightly better but the graph has a poorer performance at high temperatures. Both fits overestimate the peak position of the interaction measure. However, they both describe exactly the maximum height of the lattice data but they differ in the high temperature behavior since fit 1 decreases faster.

To achieve a better description of the lattice data, it was analyzed if a different definition of $T_{c,lattice}$ yields better fit results. For fit 1 and 2, T_c was determined as the inflection point of the curve $s/T^3(T)$ in the holographic model. As shown in in chapter 3, the value of this characteristic point in the lattice data is circa $160\,\text{MeV}$. However, choosing $T_{c,lattice} = 160\,\text{MeV}$ did not improve the fit results. Thus, the value $T_{c,lattice} = 150\,\text{MeV}$ was analyzed. The fit results 3 and 4 in table 4.3 correspond to this definition. In fact, the χ^2 values can be reduced. Figure 4.3 shows the related thermodynamic quantities. As fit 1 and 2, they can well describe the entropy density and the pressure. In addition, the speed of sound is better reproduced in the temperature range $1.3 < T/T_c < 1.6$ and the peak position and value of the interaction measure are in good agreement with the lattice data. Both fits differ in the high temperature behavior as before.

Table 4.3: Parameter values of the different fit procedures.

Fit	Fit quantity	γ	Δ	G_5	$\chi^2_{c_s^2}$	χ^2_{s/T^3}	T_c-type
1	c_s^2	0.6473	2.2765	0.4583	1.0762	0.2212	inflection
2	c_s^2	0.5347	3.9645	0.3828	1.2087	0.4272	inflection
3	c_s^2	0.6571	2.4953	0.4595	0.4663	0.1441	inflection
4	c_s^2	0.5365	3.9634	0.3922	0.4903	0.1574	inflection
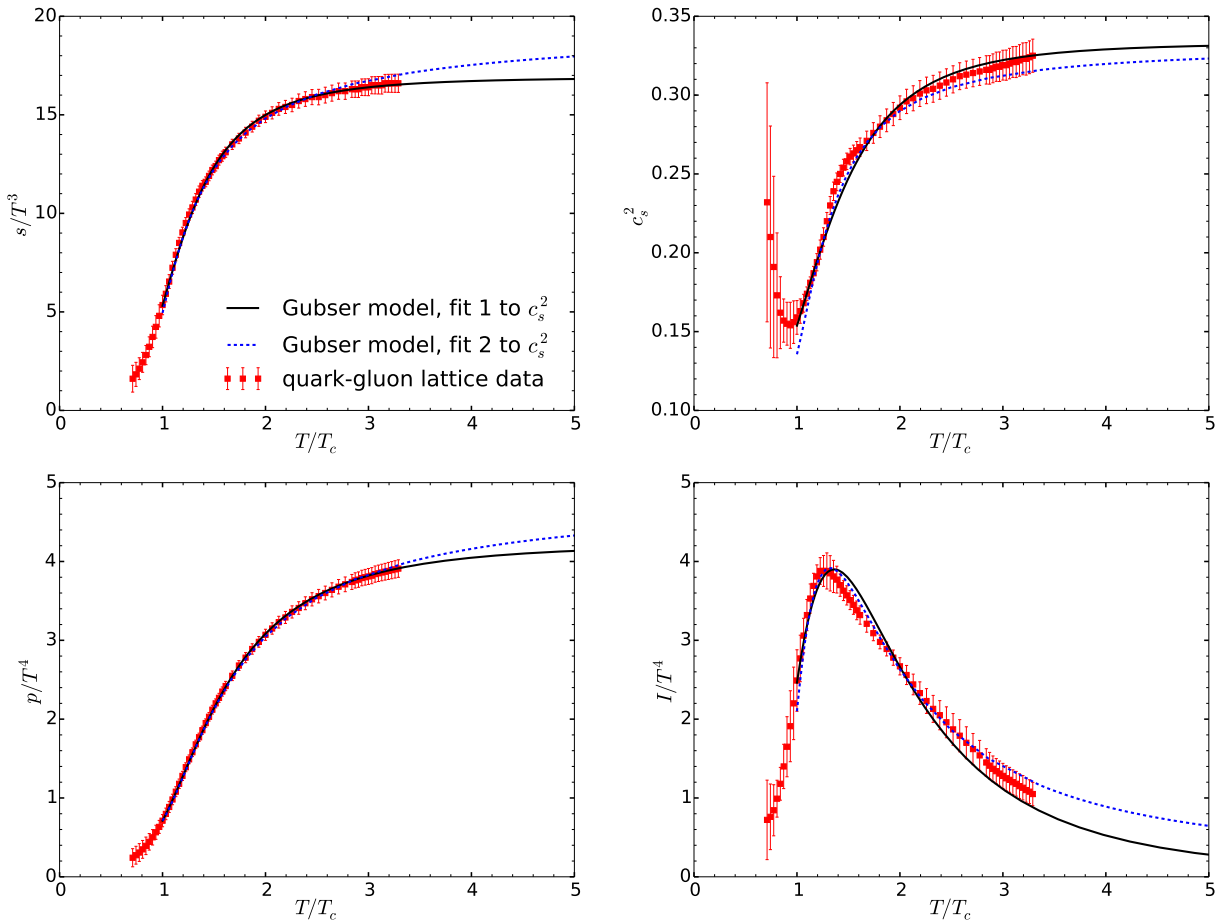
Figure 4.2: Equation of state and thermodynamic quantities of the QGP. The Gubser model is fitted to the lattice QCD data [11] with $T_{c,lattice} \equiv 155\,\mathrm{MeV}$.
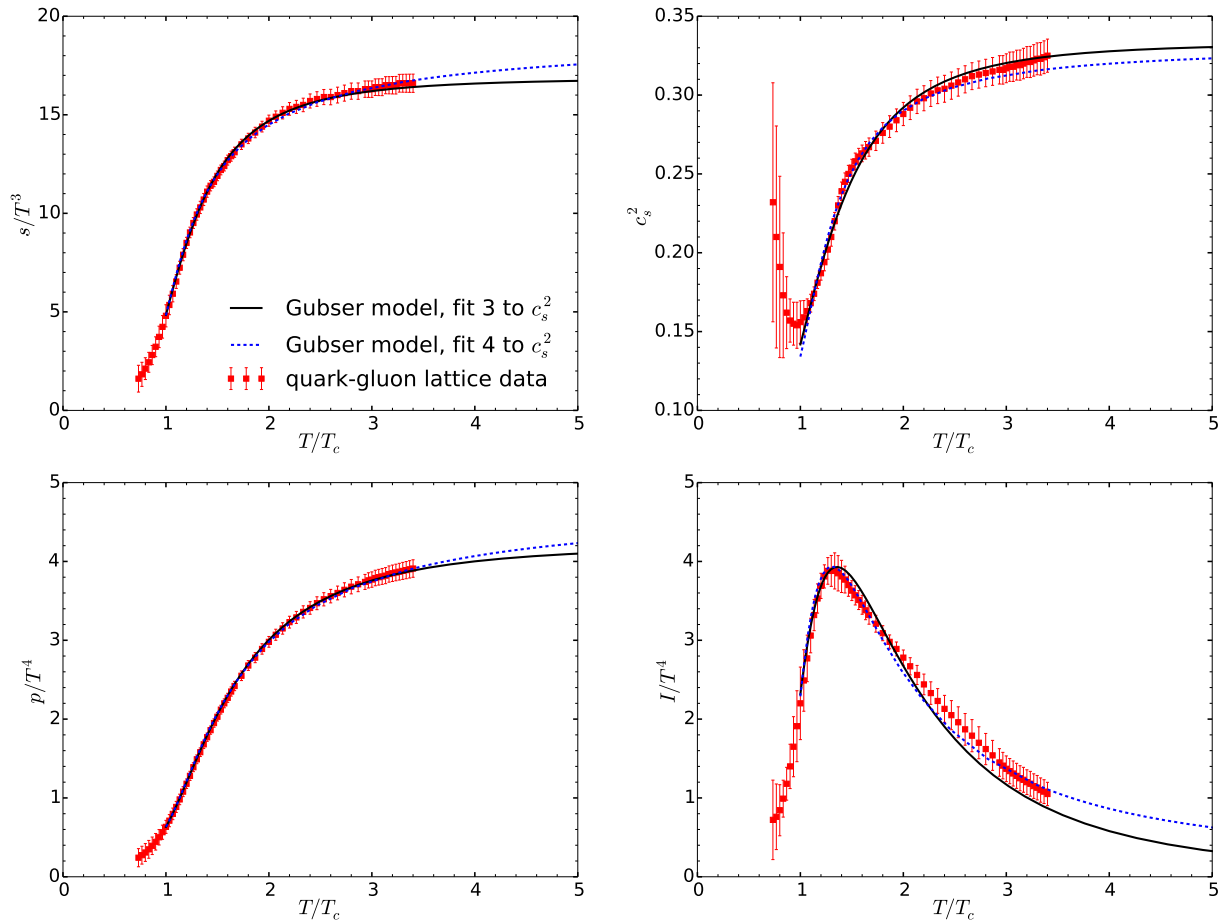
Figure 4.3: Equation of state and thermodynamic quantities of the QGP. The Gubser model is fitted to the lattice QCD data [11] with $T_{c,lattice} \equiv 150\,\text{MeV}$.

In summary it can be stated that the Gubser model allows a good description of the equation of state of the quark gluon plasma and related thermodynamic quantities in a limited temperature range. It needs to be stressed that the lattice data should be considered within their uncertainty, because the lattice data points itself are underestimated as well as overestimated in specific temperature ranges.

5 Summary and Outlook

Within the frame of this work, we have studied the equation of state of the quark gluon plasma. At first we evaluated the lattice data results from the Wuppertal-Budapest and the hotQCD collaboration (see chapter 3). The results of both collaborations agree very well. We used the lattice data from the Wuppertal-Budapest collaboration, which are calculated in the temperature range 110-510 MeV, for the holographic reconstruction of the QCD equation of state. The confinement-deconfinement transition occurs as a crossover. However, to set an absolute scale for the fit procedure, we defined the deconfinement temperature $T_c = 155$ MeV in accordance with both collaborations.

In chapter 4, we introduced two holographic models, following the work of Kiritsis and Gubser. Both models employ 5-dimensional Einstein gravity coupled to a scalar field with a non-trivial potential $V(\phi)$ to calculate the equation of state $s(T)$. We tested different procedures to fit the potential parameters. Concerning the Kiritsis model, tables 4.1 and 4.2 summarize the parameter sets. The corresponding graphs of the holographic model are shown in figure 4.1. Within the Kiritsis model, we defined T_c as the minimum of the curve $T(\phi_h)$. It is found that the Kiritsis model does not allow a good reconstruction of the QCD equation of state. Particularly, the (scaled) entropy density, speed of sound and the interaction measure are not reproduced well. The reason seems to be the fact, that the Kiritsis model is adjusted to the pure gluon plasma, which is characterized by a first-order phase transition (and not a crossover). Thus, we tested if an additional fit parameter in the potential (4.7) yields better results. In fact, no improvement can be achieved. In contrast, the Gubser model allows a good reconstruction of the equation of state of the quark-gluon plasma. In this holographic model, T_c is defined as the inflection point of the curve $s/T^3(T)$. We found two parameter sets that differ in their high temperature behavior. Table 4.3 and figure 4.2 show the results. In the temperature range $1 \leq T/T_c \lesssim 3.5$ the entropy density and pressure can be quantitatively described very well. The speed of sound and interaction measure cannot be reproduced in the whole temperature range.

A crossover has no unique transition temperature, e.g. the Wuppertal-Budapest collaboration specifies the range 150-170 MeV for the transition. However, this range allows the definition of different T_c values that are necessary for the fit procedure. In a further study, we defined $T_c = 155$ MeV for the lattice data and repeated the fit procedure of the Gubser model. In fact, this definition slightly improves the fit result. Figure 4.3 shows the equation of state and

related thermodynamic quantities for this setup.

In summary, it can be found that the Gubser model allows the reconstruction of the QCD equation of state and related thermodynamic quantities in a limited temperature range within the uncertainties of the lattice data.

In future studies we will deal with the problem of avoiding any T_c definitions, since the characteristic crossover has no unique transition temperature. An idea is to employ the parameter L, that appears in the temperature (4.19) in the holographic model, to set an absolute scale. Thus, we will fit the holographic model to the temperature of the lattice data, which is given in physical units. The advantage would be to reconstruct the equation of state in the whole temperature range of the lattice data. We have already started these studies, but have so far no results. In addition, we will calculate the shear and bulk viscosity in the holographic model.

A Detailed calculations of the Gubser model

In this chapter some more detailed calculations of the Gubser model are presented, based on [10, 39, 40]. The relevant action is

$$S = \frac{1}{16\pi G_5} \int d^5x \sqrt{-g}\,(R + \mathcal{L}_M) \tag{A.1}$$

with

$$\mathcal{L}_M = -\frac{1}{2}\partial_\mu\phi\partial^\mu\phi - V(\phi) = -\frac{1}{2}\partial_\mu\phi\partial_\nu\phi\, g^{\mu\nu} = \mathcal{L}_M(g^{\mu\nu})\;. \tag{A.2}$$

The field equations follow from

$$R_{\mu\nu} - \frac{1}{2}R g_{\mu\nu} = T_{\mu\nu} \tag{A.3}$$

with the ansatz for the metric

$$ds^2 = e^{2A(\phi)}\left(-f(\phi)dt^2 + d\vec{x}^2\right) + \frac{L^2}{f(\phi)}e^{2B(\phi)}d\phi^2\;. \tag{A.4}$$

The numbering scheme is $(t, x^1, x^2, x^3, \phi) = (x^0, x^1, x^2, x^3, x^5)$. In a five dimensional curved space, the energy-momentum tensor follows from

$$
\begin{aligned}
T_{\mu\nu} &= -\frac{1}{\sqrt{-g}}\frac{\delta(\sqrt{-g}\mathcal{L}_M)}{\delta g^{\mu\nu}} \\
&= -\frac{1}{\sqrt{-g}}\left(\mathcal{L}_M\frac{\delta\sqrt{-g}}{\delta g^{\mu\nu}} + \sqrt{-g}\frac{\delta\mathcal{L}_M}{\delta g^{\mu\nu}}\right) \quad\Bigg|\quad \delta\sqrt{-g} = -\frac{\sqrt{-g}}{2}g_{\mu\nu}\delta g^{\mu\nu} \\
&= -\frac{1}{\sqrt{-g}}\left(-\mathcal{L}_M\frac{\sqrt{-g}}{2}g_{\mu\nu}\frac{\delta g^{\mu\nu}}{\delta g^{\mu\nu}} + \sqrt{-g}\frac{\delta\mathcal{L}_M}{\delta g^{\mu\nu}}\right) \\
&= -\left(-\frac{\mathcal{L}_M}{2}g_{\mu\nu} + \frac{\delta\mathcal{L}_M}{\delta g^{\mu\nu}}\right) \\
&\overset{(A.2)}{=} -\frac{1}{4}\partial_\mu\phi\partial^\mu\phi\, g_{\mu\nu} - \frac{1}{2}V(\phi)g_{\mu\nu} - \frac{\partial\mathcal{L}_M}{\partial g^{\mu\nu}} \\
&\overset{(A.2)}{=} -\frac{1}{4}(\partial\phi)^2 g_{\mu\nu} - \frac{1}{2}V(\phi)g_{\mu\nu} + \frac{1}{2}\partial_\mu\phi\partial_\nu\phi\;,
\end{aligned}
\tag{A.5}
$$

with the components

$$
T_{00} = -\frac{1}{2}V g_{00} = \frac{1}{2}V e^{2A} f \ , \qquad T_{11} = T_{22} = T_{33} = -\frac{1}{2}V g_{11} = -\frac{1}{2}V e^{2A} \ ,
$$
$$
T_{55} = -\frac{1}{4}g_{55} - \frac{1}{2}V g_{55} + \frac{1}{2} = -\frac{1}{4}\frac{L^2}{f}e^{2B} - \frac{1}{2}V\frac{L^2}{f}e^{2B} + \frac{1}{2} = -\frac{1}{2}\frac{L^2}{f}e^{2B}\left(\frac{1}{2} + V\right) + \frac{1}{2} \ . \tag{A.6}
$$

Using a computer algebra system, one derives the Einstein equations (A.3)

$$
A'' - A'B' + \frac{1}{6} = 0 \ , \tag{A.7}
$$

$$
\frac{f''}{f'} = -4A' + B' \ , \tag{A.8}
$$

$$
6A'\frac{f'}{f} + \left(24A'^2 - 1\right) = -\frac{2}{f}e^{2B}L^2V \ . \tag{A.9}
$$

The first two of these equations follow from the (00) and (11) components; the third comes from the (55) component.[22] The scalar equation of motion for ϕ comes from[23]

$$
T^{\mu\nu}_{\ \ ;\nu} = 0 \quad \Rightarrow \quad 4A' - B' + \frac{f'}{f} = \frac{e^{2B}}{f}L^2V' \ . \tag{A.10}
$$

To transform the eqs. (A.7)–(A.10) into scalar equations, we define

$$
g' = (\ln f)' = \frac{f'}{f} \ . \tag{A.11}
$$

It follows

$$
g'' = \frac{f''f - f'f'}{f^2} = \frac{f''}{f} - g'^2 \qquad \Big| \cdot \frac{f}{f'}
$$
$$
\frac{g''f}{f'} = \frac{f''}{f'} - \frac{f'}{f} \quad \Rightarrow \quad \frac{f''}{f'} = \frac{g''}{g'} + g'. \tag{A.12}
$$

Dividing (A.10) by (A.9) yields

$$
-\frac{V'}{2V} = \frac{4A' - B' + \dfrac{f'}{f}}{6A'\dfrac{f'}{f} + 24'^2 - 1} \overset{(A.7)}{=} \frac{4A' - \left(\dfrac{A''}{A'} + \dfrac{1}{6A'}\right) + \dfrac{f'}{f}}{6A'\dfrac{f'}{f} + 24'^2 - 1} \overset{(A.11)}{=} \frac{4A' - \dfrac{A''}{A'} - \dfrac{1}{6A'} + g'}{6A'g' + 24'^2 - 1}
$$

$$
= \frac{1}{6A'} \cdot \frac{4A' - \dfrac{A''}{A'} - \dfrac{1}{6A'} + g'}{g' + 4' - \dfrac{1}{6A'}} \ . \tag{A.13}
$$

---

[22] A prime denotes a derivative w.r.t. ϕ.

[23] This relation is sometimes also denoted as $\Box\phi = V'(\phi)$ and not independent.

This relation is equivalent to

$$-\frac{3A'V'}{V} = 1 + \frac{A''}{-g'A' - 4A'^2 + \frac{1}{6}} = 1 + \frac{A''}{-4A'^2\left(\frac{g'}{4A'} + 1 - \frac{1}{24A'^2}\right)} \tag{A.14}$$

and finally

$$-\frac{A''}{4A'^2} = -\left(\frac{3A'V'}{V} + 1\right)\left(\frac{g'}{4A'} + 1 - \frac{1}{24A'^2}\right) . \tag{A.15}$$

On the other hand, we replace B' in (A.8) using (A.7) and obtain

$$\frac{f''}{f'} \overset{\text{(A.12)}}{=} \frac{g''}{g'} + g' = -4A' + \frac{A''}{A'} + \frac{1}{6A'} \quad \Big| \cdot \frac{g'}{A'} \tag{A.16}$$

$$\Leftrightarrow \frac{g''}{A'} + \frac{g'^2}{A'} = -4g' + \frac{g'A''}{A'^2} + \frac{g'}{6A'^2} \tag{A.17}$$

$$\Leftrightarrow \frac{g''}{4A'} - \frac{g'A''}{4A'^2} = -\left(1 + \frac{g'}{4A'} - \frac{1}{24A'^2}\right)g'. \tag{A.18}$$

We define

$$X \equiv \frac{1}{4A'} , \tag{A.19}$$

$$Y \equiv \frac{g'}{4A'} . \tag{A.20}$$

Plugging (A.19) into (A.15) and (A.20) into (A.18), we obtain the final result for the scalar equations

$$X' = -\left(1 + Y - \frac{2}{3}X^2\right)\left(1 + \frac{3V'}{4XV}\right) , \tag{A.21}$$

$$Y' = -\left(1 + Y - \frac{2}{3}X^2\right)\frac{Y}{X} . \tag{A.22}$$

The Hawking temperature is calculated using the formula

$$T = \frac{\varkappa}{2\pi}\Big|_h = \frac{g_{tt,r}}{4\pi\sqrt{-g_{tt}g_{rr}}}\Big|_{r=r_h} , \tag{A.23}$$

where $\varkappa$ is the surface gravity at the black hole horizon and r stands for the radial coordinate of the metric. In the approach by Gubser, we have $g_{00} = -e^{2A}f$ and $g_{55} = \frac{L^2}{f}e^{2B}$. It follows $\sqrt{-g_{tt}g_{rr}} = \sqrt{-g_{00}g_{55}} = Le^{A+B}$ and $g_{tt,r} = g_{00,5} = e^{2A}\left(-2A'f - f'\right)$. This leads to

$$T = \frac{1}{4\pi}\left[\frac{e^{2A}\left(-2A'f - f'\right)}{Le^{A+B}}\right]\Big|_{\phi_h} . \tag{A.24}$$

Due to the boundary condition $f(\phi_h) = 0$, we finally obtain

$$TL = -\frac{1}{4\pi} f' e^{A-B}\bigg|_{\phi_h} . \tag{A.25}$$

B Holographic description of the gluon plasma

This chapter summarizes previous studies, whose aim was a holographic description of the pure gluon plasma. In fact, the Kiritsis model (see section 4.1) was used to calculate the equation of state and viscosities. The lattice data for the fit procedure originated from [28]. The focus lies on the description of the temperature range $1 \leq T/T_c \leq 10$. The main difference to the QGP is the appearance of of a first-order deconfinement phase transition.

The fit procedure was performed in the same way as for the QGP with the definition

$$\chi_q^2 = \ln \left(10^3 \frac{1}{\ln N} \sum_{i=1}^{N} \left[q_h(\ln \frac{T_i}{T_c}) - q_L(\ln \frac{T_i}{T_c}) \right]^2 \right) \tag{B.1}$$

and the parameter value $P = 1/2$. We considered different versions of the Kiritsis model: First, the so-called *original* model. In this setup, the free energy (density) is calculated as

$$\frac{F}{V}(\lambda_h) = \int_{\lambda_h}^{\infty} s(\bar{\lambda}_h) \frac{dT(\bar{\lambda}_h)}{d\bar{\lambda}_h} d\bar{\lambda}_h \ . \tag{B.2}$$

The pressure is related to the free energy through the relation $p = -\partial F/\partial V = -F/V$ and T_c is defined as $T_c \equiv T(\lambda_c)$ whereby λ_c is the zero of the function $p(\lambda_h)$. The other thermodynamic quantities are calculated with the relations in (4.11) with $p_0 = 0$. The fit parameters for the potential are taken from [31]. In addition, we fitted this original setup to the more recent lattice data [28].[24] In this case, $p_0 = p(T_c)$ is taken from these lattice data. As a third method, we defined T_c as the minimum of the curve $T(\lambda_h)$ and calculated the other quantities as before. This setup is denoted as *improved* in the following.

The two different fit procedures, which are described in section 4.1, were also applied here. Figure B.1 summarizes the results for a fit to the speed of sound and figure B.2 shows the results for a fit to the entropy density. The numerical results are summarized in table B.1.

As can be seen from the figures, the original model does not allow a good description of the lattice data. The speed of sound, pressure and entropy density are overestimated in the temperature range $1 \leq T/T_c \leq 2$, whereas the pressure and entropy density are underestimated in

---

[24]The original setup in [31] was fitted to the older lattice data [29].

Table B.1: Parameter values of the different fit procedures for the Kiritsis model.

Fit	Type	Fit quantity	V_1	V_3	G_5	$\chi^2_{c_s^2}$	χ^2_{s/T^3}	T_c-type
1	original		14	170	1.104	-0.169	4.896	zero
2	original new fit	c_s^2	6.079	176.573	1.011	-1.213	4.474	zero
3	improved	c_s^2	13.113	180.078	1.069	-5.138	1.914	minimum
4	original new fit	s/T^3	10.998	199.970	1.064	-0.792	4.140	zero
5	improved	s/T^3	12.977	180.990	1.068	-5.122	1.910	minimum

the range $2 \leq T/T_c \leq 10$. However, the high temperature behavior of the interaction measure is well described. In fact, the fit of the original model to the new lattice data marginally reduces the χ^2-value. In case of the fit to the speed of sound (number 2 in table B.1), the new fit overestimates the lattice data in opposite manner than the original model. If the original model is fitted to the entropy density (fit 4), the result is much better, as may be seen from figure B.2. This fit slightly overestimates the c_s^2-lattice data in the range $1 \leq T/T_c \leq 2$. The peak height of the interaction measure is well described in contrast to the high temperature behavior. The improved Kiritsis model allows the best description of the lattice data (fit 3 and 5). The χ^2 values are significantly reduced. Furthermore, one can assume that the fits to c_s^2 and s/T^3 converge to the same parameters for V_1, V_3 and G_5. The lattice data of the speed of sound, pressure and entropy density are described nearly perfectly. Only the high temperature behavior of the interaction measure is not as good as that of the original model.

In the following, the improved Kiritsis model (fit 5) is compared to the Gubser model (see section 4.2). The optimal fit parameters of the Gubser model, which describe the gluon plasma, are taken from [41]. We calculated with $\gamma = 0.6938$, $\Delta = 3.5976$ and $G_5 = 1.1753$. T_c is defined as the minimum of the curve $T(\phi_h)$ in this model. The resulting χ^2 values are $\chi^2_{c_s^2} = -4.4595$ and $\chi^2_{s/T^3} = 1.1555$.

Figure B.3 shows the potential of the optimal fits in dependence of the variable ϕ_G that appears in the Gubser model (see (4.18)) as the holographic coordinate. The variable $\phi_K \equiv \Phi$, appearing in the Kiritsis model (4.7), follows from the relation $\phi_G = \phi_K \sqrt{8/3}$. The difference arises because of the different factors in the action for the Kiritsis (4.1) and Gubser model (4.13). The ϕ_G-interval is chosen so that the temperature range $1 \leq T/T_c \leq 10$ is described exactly. The minimum value of ϕ_G corresponds to $10\,T_c$. Since the ϕ_G values are negative in the Kiritsis model, the curve is shifted such that the minimal values match with the Gubser model. Remarkably, the original and improved Kiritsis model do not differ much, although they describe the lattice data very differently.[25] In contrast, the potential of the Gubser model extends in a wider range of values. Although the two models use totally different potential approaches, both models allow the description of the lattice data. The right plot in figure B.3 shows the ratio of the derivative of the potential $(dV(\phi_G)/d\phi_G)$ to the potential. In case of the

---

[25]For comparison with the Gubser model, $-V_K(\phi_G)$ is plotted.
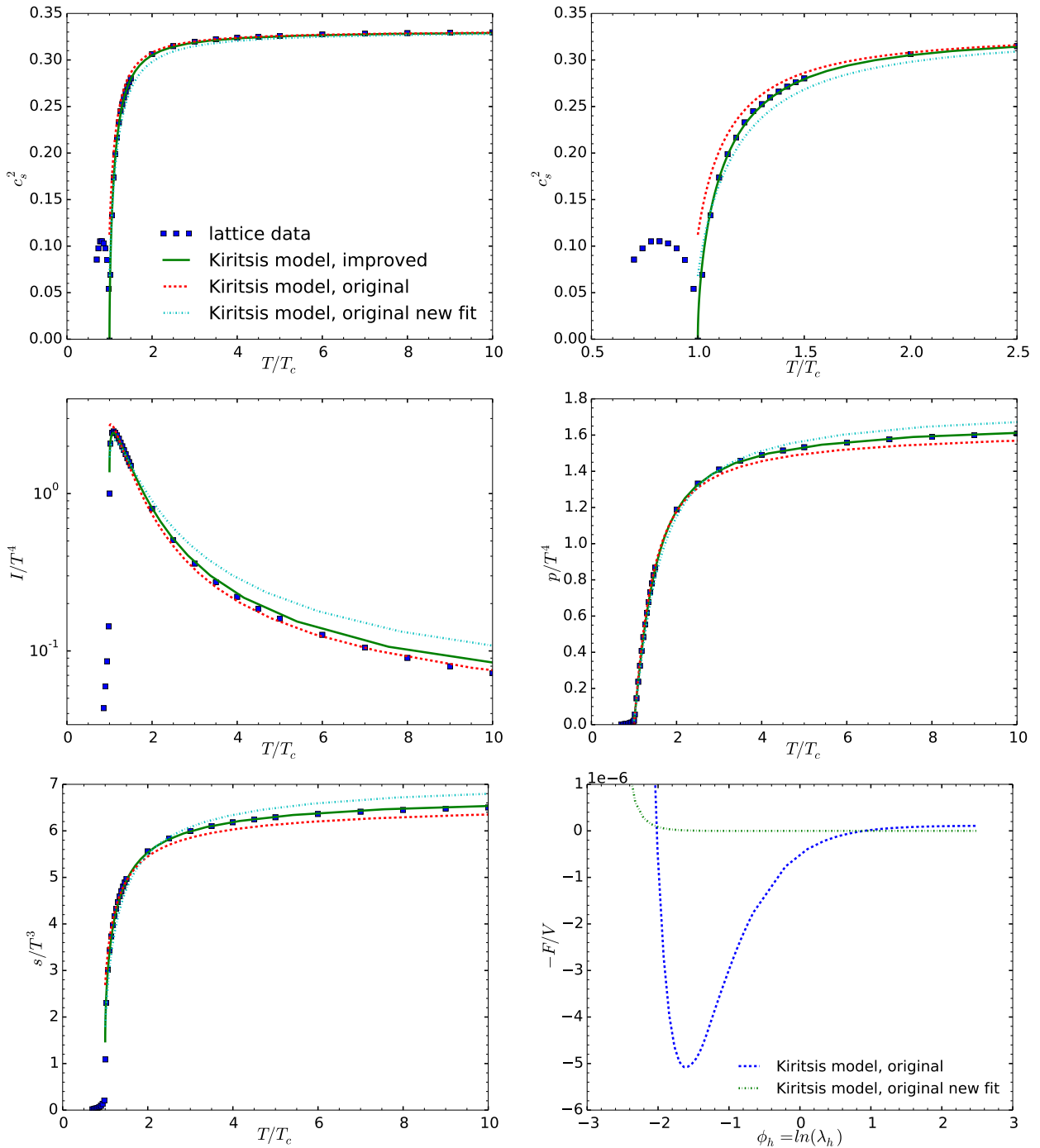
Figure B.1: Equation of state and thermodynamic quantities of the pure gluon plasma. Squares: lattice data [28]. The Kiritsis model is primary fitted to the speed of sound c_s^2.

Kiritsis model, the derivative is calculated as $\frac{dV(\lambda(\phi_G))}{d\phi_G} = \frac{dV(\lambda)}{d\lambda}\frac{d\lambda}{d\phi_G}$. The slopes of the curves do not match exactly.

Figure B.4 shows the speed of sound end entropy density of the two models. The two models are in good agreement with the lattice data in the studied temperature range. In more detail, the entropy density is very slightly underestimated in the temperature range $1.1 \leq T/T_c \leq 3.5$ in the Kiritsis model and very slightly overestimated in the Gubser model in this range. For
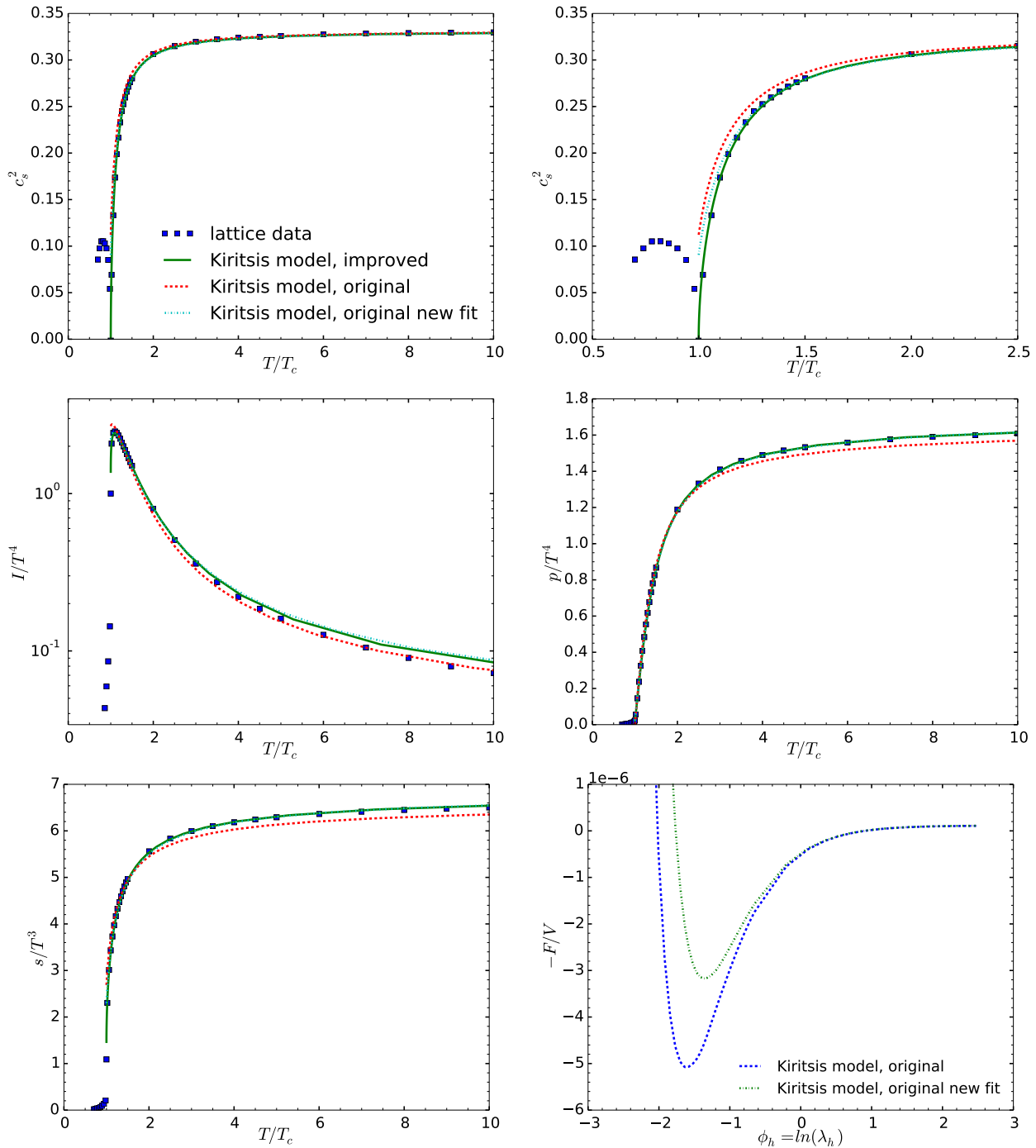
Figure B.2: Equation of state and thermodynamic quantities of the pure gluon plasma. Squares: lattice data [28]. The Kiritsis model is fitted to the entropy density s/T^3.

higher temperatures, the situation is reversed.

Furthermore, we studied the viscosities of the gluon plasma. Namely, the relevant quantities are the bulk- ζ and shear viscosity η. The shear viscosity is holographically calculated by the relation [42]

$$\eta = \frac{s}{4\pi} \ . \tag{B.3}$$

The ratio of bulk to shear viscosity is calculated with the formula of Elling and Oz [43]. The
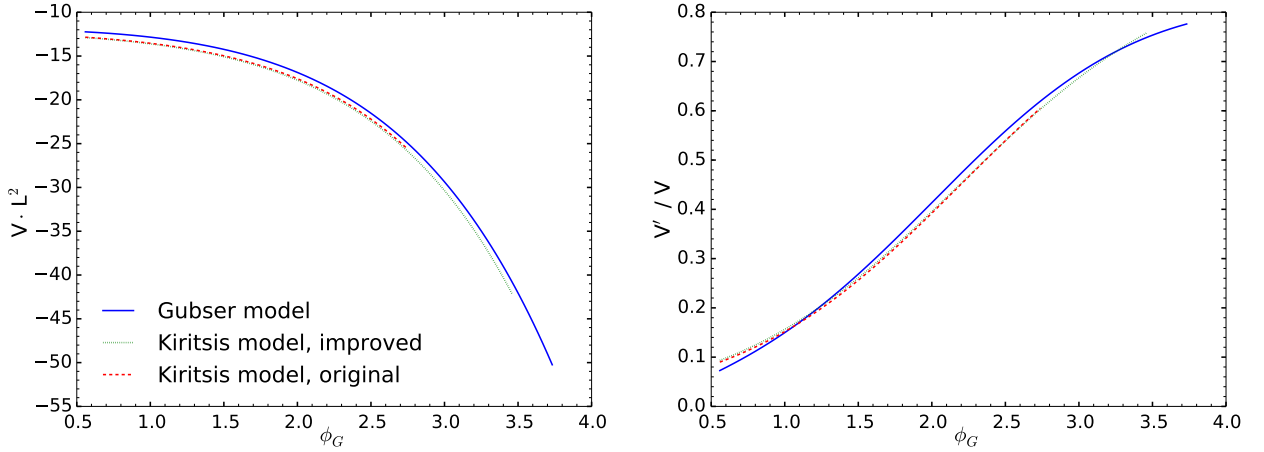
Figure B.3: Potential of the improved and original Kiritsis model in comparison to the Gubser model. The parameter values from the Gubser model are taken from [41].
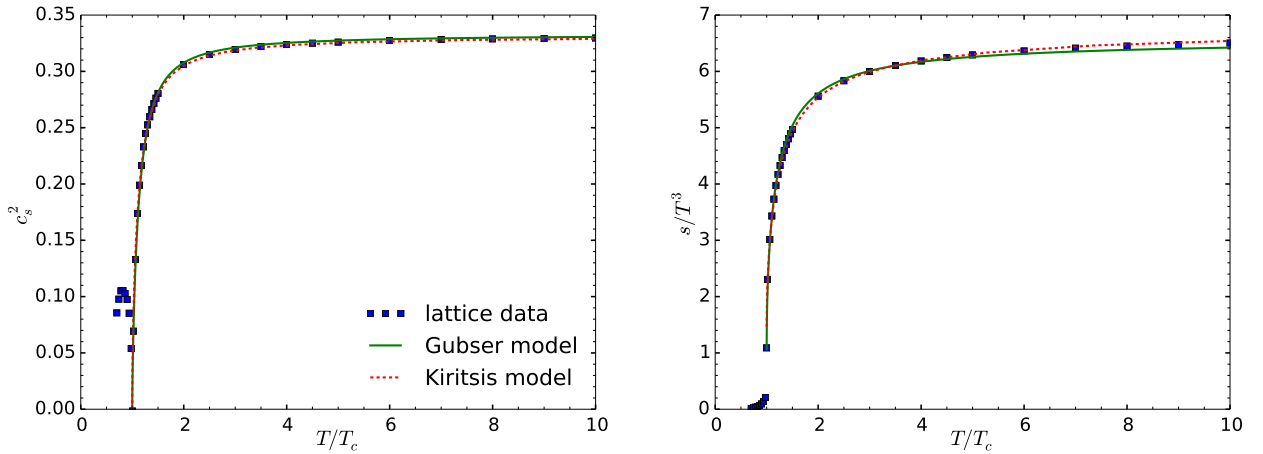

Figure B.4: Speed of sound and entropy density of the improved Kiritsis model in comparison to the Gubser model. The parameter values from the Gubser model are taken from [41].

most general form reads as follows

$$\frac{\zeta}{\eta} = \sum_i \left(s \frac{d\phi_{i,h}}{ds} + \rho^a \frac{d\phi_{i,h}}{d\rho^a} \right)^2 \ . \tag{B.4}$$

Here, ρ^a are the charges associated with the gauge fields A_μ^a that appear in the action. Specifically, the equations for the Gubser and Kiritsis model are

$$\frac{\zeta}{\eta} = \left(\frac{\mathrm{d} \ln(s)}{\mathrm{d}\phi_h} \right)^{-2} \ . \tag{B.5}$$

Figure B.5 shows the results of the analysis. The ratio of bulk to shear viscosity is plotted in dependence of the scaled temperature and the non-conformality measure. The latter one is

defined as[26]

$$\Delta c_s^2 = \frac{1}{3} - c_s^2 \ . \tag{B.6}$$

The ratio of the viscosities displays a nearly linear section in the range $0 \leq \Delta c_s^2 \leq 0.24$, which was already described in [44] for the Gubser model. The improved Kiritsis model confirms this result. However, there occur deviations for high values of Δc_s^2, which correspond to values close by the critical temperature T_c. (The differences for high temperatures, that occur in the double logarithmic plot on the right side of figure B.5 are negligible.)
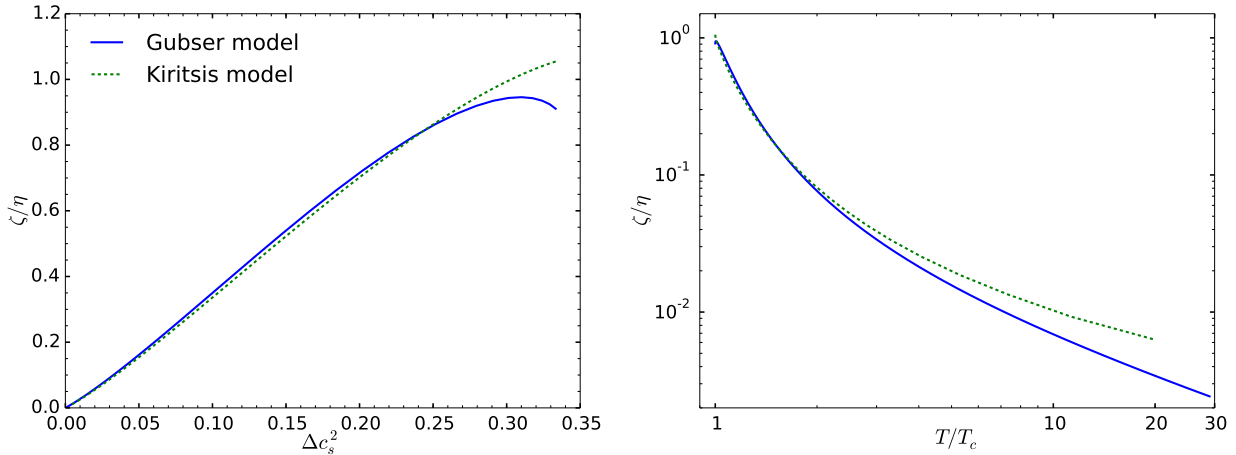
Figure B.5: Ratio of bulk to shear viscosity of the improved Kiritsis model in comparison to the Gubser model. The parameter values from the Gubser model are taken from [41].

Remarkably, these differences correspond to the very small temperature interval $1.00 \leq T/T_c \leq 1.03$. To analyze possible reasons for this behavior, figure B.6 compares the equation of state, i.e. the temperature and entropy density, in dependence of ϕ_G (w.r.t. the Gubser model) for both models. Since the ratio of the viscosities is calculated from the entropy, differences in the curves directly influence the viscosities. Note that high values of ϕ_G correspond to small temperatures. In fact, the graphs $\ln s(\phi_G)$ do not differ much. However, two intersection points at $\phi_G \approx 0.7$ and $\phi_G \approx 1.9$ imply that even very small differences in the slope of the curves cause the differences in the viscosities. Therefore, the logarithmic derivative of the entropy density is shown in figure B.7. There occur very small differences for high values of ϕ_G. Moreover, the graph of the Gubser model exhibits a local maximum at $\phi_G \approx 3.34$, which corresponds to an inflection point in the curve $\ln s(\phi_G)$ in figure B.6. Since the improved Kiritsis model does not exhibit this behavior, there occur differences in the ratio of the viscosities.

---

[26]The name refers to the fact, that for an ideal gas the relation $\Delta c_s^2 = 0$ holds.
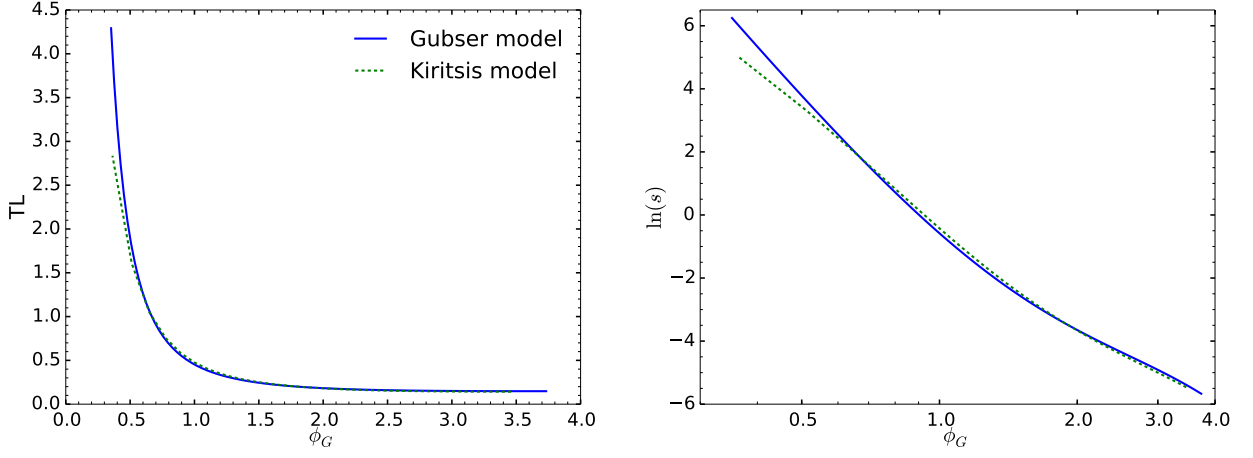
Figure B.6: Temperature and entropy of the improved Kiritsis model in comparison to the Gubser model. The graph of the Kiritsis model is shifted so that the values ϕ_G that correspond to $T/T_c = 10$ are superimposed. The parameter values from the Gubser model are taken from [41].
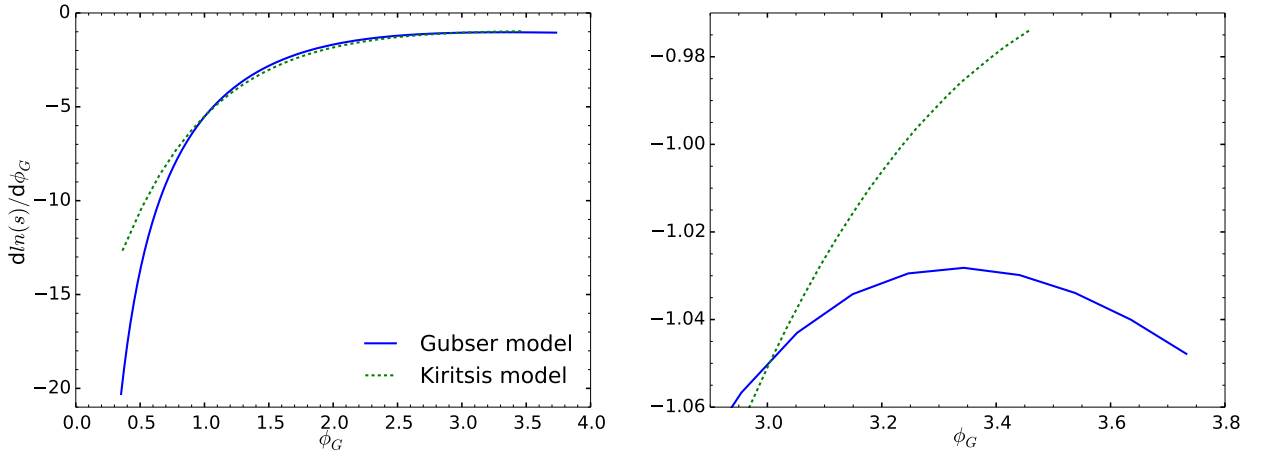

Figure B.7: Logarithmic derivative of the entropy density. The graph of the Kiritsis model is shifted so that the values ϕ_G that correspond to $T/T_c = 10$ are superimposed. The parameter values from the Gubser model are taken from [41].

Bibliography

[1] T. Fließbach, Allgemeine Relativitätstheorie, 6th Edition, Springer Spektrum, 2012.

[2] P. Raschewski, Riemannsche Geometrie und Tensoranalysis, VEB Deutscher Verlag der Wissenschaften, 1959.

[3] D. Hilbert, Die Grundlagen der Physik. Erste Mitteilung, Nachr. v. d. Kgl. Ges. d. Wiss. z. Göttingen, Math.-phys. Klasse 27 (1915) 395–407.
URL `http://echo.mpiwg-berlin.mpg.de/content/modernphysics/hilbert`

[4] R. U. Sexl, H. K. Urbantke, Gravitation und Kosmologie, 4th Edition, Spektrum Akademischer Verlag, 1995.

[5] H. Goenner, Einführung in die spezielle und allgemeine Relativitätstheorie, Spektrum Akademischer Verlag, 1996.

[6] T. Muta, Foundations of Quantum Chromodynamics, 2nd Edition, World Scientific Publishing Co. Pte. Ltd., 1998.

[7] A. Straessner, S. Lammers, Nuclear- and particle physics, University Lecture (Dresden University of Technology) (2013).

[8] University of Jyväskylä, Department of Physics, Ordinary strong interactions: QCD phase diagrams, `https://www.jyu.fi/fysiikka/en/research/highenergy/parphen/QCD`, Accessed: 09/03/2014.

[9] N. Cabibbo, G. Parisi, Exponential Hadronic Spectrum and Quark Liberation, Phys. Lett. B 59 (1975) 67–69. `doi:10.1016/0370-2693(75)90158-6`.

[10] R. Yaresko, Equation of state and viscosities of the gluon plasma in a holographic approach, Diploma thesis, Dresden University of Technology (2013).

[11] S. Borsanyi, Z. Fodor, C. Hoelbling, S. D. Katz, S. Krieg, et al., Full result for the QCD equation of state with 2+1 flavors, Phys. Lett. B 730 (2014) 99–104. `arXiv:1309.5258`, `doi:10.1016/j.physletb.2014.01.007`.

[12] S. Borsanyi, et al., Is there still any T_c mystery in lattice QCD? Results with physical masses in the continuum limit III, JHEP 1009 (2010) 073. `arXiv:1005.3508, doi:10.1007/JHEP09(2010)073`.

[13] W. Unger, The Chiral Phase Transition in QCD: on the quark mass dependence of Goldstone fluctuations, Slides of a talk given at Δ Meeting - Heidelberg, January 31 (2009).

[14] R. J. Szabo, BUSSTEPP lectures on string theory: An Introduction to string theory and D-brane dynamics `arXiv:hep-th/0207142`.

[15] H. Nastase, Introduction to AdS-CFT `arXiv:0712.0689`.

[16] K. Becker, M. Becker, J. Schwarz, String Theory and M-Theory: A Modern Introduction, Cambridge University Press, 2007.

[17] K. Hashimoto, D-Brane: Superstrings and New Perspective of Our World, Springer-Verlag, 2012.

[18] E. D'Hoker, D. Phong, Lectures on supersymmetric Yang-Mills theory and integrable systems (1999) 1–125 `arXiv:hep-th/9912271`.

[19] J. M. Maldacena, The Large N limit of superconformal field theories and supergravity, Int. J. Theor. Phys. 38 (1999) 1113–1133. `arXiv:hep-th/9711200, doi:10.1023/A:1026654312961`.

[20] S. Gubser, I. R. Klebanov, A. M. Polyakov, Gauge theory correlators from noncritical string theory, Phys. Lett. B 428 (1998) 105–114. `arXiv:hep-th/9802109, doi:10.1016/S0370-2693(98)00377-3`.

[21] E. Witten, Anti-de Sitter space and holography, Adv. Theor. Math. Phys. 2 (1998) 253–291. `arXiv:hep-th/9802150`.

[22] B. Kämpfer, Applied string theory, University Lecture (Dresden University of Technology) (2013).

[23] J. Polchinski, Dirichlet Branes and Ramond-Ramond charges, Phys. Rev. Lett. 75 (1995) 4724–4727. `arXiv:hep-th/9510017, doi:10.1103/PhysRevLett.75.4724`.

[24] H. Nastase, Introduction to Supergravity `arXiv:1112.3502`.

[25] O. Aharony, S. S. Gubser, J. M. Maldacena, H. Ooguri, Y. Oz, Large N field theories, string theory and gravity, Phys. Rept. 323 (2000) 183–386. `arXiv:hep-th/9905111, doi:10.1016/S0370-1573(99)00083-6`.

[26] P. Weisz, P. Majumdar, Lattice gauge theories, Scholarpedia 7 (4) (2012) 8615.

[27] A. Bazavov, The QCD equation of state, Slides of a talk given at the XXIV Quark Matter conference, May 20 (2014).

[28] S. Borsanyi, G. Endrodi, Z. Fodor, S. Katz, K. Szabo, Precision SU(3) lattice thermodynamics for a large temperature range, JHEP 1207 (2012) 056. `arXiv:1204.6184`, `doi:10.1007/JHEP07(2012)056`.

[29] G. Boyd, J. Engels, F. Karsch, E. Laermann, C. Legeland, et al., Thermodynamics of SU(3) lattice gauge theory, Nucl. Phys. B 469 (1996) 419–444. `arXiv:hep-lat/9602007`, `doi:10.1016/0550-3213(96)00170-8`.

[30] S. S. Gubser, A. Nellore, Mimicking the QCD equation of state with a dual black hole, Phys. Rev. D 78 (2008) 086007. `arXiv:0804.0434`, `doi:10.1103/PhysRevD.78.086007`.

[31] U. Gursoy, E. Kiritsis, L. Mazzanti, F. Nitti, Improved Holographic Yang-Mills at Finite Temperature: Comparison with Data, Nucl. Phys. B 820 (2009) 148–177. `arXiv:0903.2859`, `doi:10.1016/j.nuclphysb.2009.05.017`.

[32] U. Gursoy, E. Kiritsis, Exploring improved holographic theories for QCD: Part I, JHEP 0802 (2008) 032. `arXiv:0707.1324`, `doi:10.1088/1126-6708/2008/02/032`.

[33] U. Gursoy, E. Kiritsis, F. Nitti, Exploring improved holographic theories for QCD: Part II, JHEP 0802 (2008) 019. `arXiv:0707.1349`, `doi:10.1088/1126-6708/2008/02/019`.

[34] U. Gursoy, E. Kiritsis, L. Mazzanti, F. Nitti, Holography and Thermodynamics of 5D Dilaton-gravity, JHEP 0905 (2009) 033. `arXiv:0812.0792`, `doi:10.1088/1126-6708/2009/05/033`.

[35] S. Hawking, Particle Creation by Black Holes, Commun. Math. Phys. 43 (1975) 199–220. `doi:10.1007/BF02345020`.

[36] J. D. Bekenstein, Black holes and entropy, Phys. Rev. D 7 (1973) 2333–2346. `doi:10.1103/PhysRevD.7.2333`.

[37] Laub, C. and Tonya, L. K., How Bad is Good?, Slides of a talk given at University of California, Davis `http://neutrons.ornl.gov/workshops/sns_hfir_users/posters/Laub_Chi-Square_Data_Fitting.pdf`, Accessed: 09/18/2014.

[38] S. S. Gubser, A. Nellore, S. S. Pufu, F. D. Rocha, Thermodynamics and bulk viscosity of approximate black hole duals to finite temperature quantum chromodynamics, Phys. Rev. Lett. 101 (2008) 131601. `arXiv:0804.1950`, `doi:10.1103/PhysRevLett.101.131601`.

[39] S. S. Gubser, S. S. Pufu, F. D. Rocha, Bulk viscosity of strongly coupled plasmas with holographic duals, JHEP 0808 (2008) 085. `arXiv:0806.0407`, `doi:10.1088/1126-6708/2008/08/085`.

[40] R. Yaresko, Scalar equations, private communication (2013).

[41] R. Yaresko, private communication (2014).

[42] P. Kovtun, D. T. Son, A. O. Starinets, Viscosity in strongly interacting quantum field theories from black hole physics, Phys. Rev. Lett. 94 (2005) 111601. `arXiv:hep-th/0405231`, `doi:10.1103/PhysRevLett.94.111601`.

[43] C. Eling, Y. Oz, A Novel Formula for Bulk Viscosity from the Null Horizon Focusing Equation, JHEP 1106 (2011) 007. `arXiv:1103.1657`, `doi:10.1007/JHEP06(2011)007`.

[44] R. Yaresko, B. Kämpfer, Bulk viscosity of the gluon plasma in a holographic approach, Acta Phys. Polon. Supp. 7 (1) (2014) 137–144. `arXiv:1403.3581`, `doi:10.5506/APhysPolBSupp.7.137`.

Acknowledgements

Erklärung

Hiermit erkläre ich, dass ich diese Arbeit im Rahmen der Betreuung am Institut für Theoretische Physik ohne unzulässige Hilfe Dritter verfasst und alle Quellen als solche gekennzeichnet habe.

Johannes Knaute

Dresden, Oktober 2014